VOLUMINA JURASSICA, 2024, XXII: 87–116
DOI: 10.7306/VJ.22.6

Timing and duration of the early Hettangian marine inundation in the Polish Basin: Organic carbon isotopes and astronomical calibration of the Triassic–Jurassic transition of the Niekłań PIG core (Holy Cross Mountains, SE Poland)

Damian G. LODOWSKI[1], Mathieu MARTINEZ[2], Stephen P. HESSELBO[3], Marta HODBOD[1], Melanie J. LENG[4], Grzegorz PIEŃKOWSKI[1]
with contribution of Paweł Brański[1] and Robyn Pointer[3]

Key words: Rhaetian, Hettangian, terrestrial succession, clay minerals, carbon isotopes, magnetic susceptibility, astrochronology, sea-level change.

Abstract. Stratigraphy of non-marine sections and dynamics of marine transgressions in the deep geological past are important, yet challenging issues. Here we discuss results obtained from the Triassic–Jurassic (T–J) boundary interval of the Niekłań PIG drillcore section (Holy Cross Mountains or HCM, SE Poland). The core represents an expanded record of continental to marginal-marine facies, deposited within the axial part of the Polish Basin. The section is dated based on an integrated approach, utilizing palynologic proxies, stable carbon isotope correlations, and astronomical tuning of the section. Palaeoenvironment and its evolution is established by means of high-resolution sedimentology, clay mineral assemblages, and geochemical weathering indices (chemical index of alteration, CIA). The early to mid-Rhaetian was seasonal and progressively warmer and more humid, culminating with a hot and humid climate in the late Rhaetian; the earliest Jurassic was slightly cooler, yet still warm and humid, with year-round rainfall. Characteristic for the T/J boundary is the occurrence of two fern spikes (uppermost Rhaetian and lowermost Hettangian), which are associated with vegetation crises; this interval is also marked by wildfire indicators. Recognition of short eccentricity (~100 kyr) cycles enables calculation of sedimentation rates as well as temporal interpretation of the early Rhaetian marine inundation onto coastal plains of the Polish Basin. To begin with, over a period of ~200 kyr, a base-level rise led in the HCM region to a shift from fluvial to lacustrine depositional systems, while the final flooding marked by the onset of marine facies took another ~350 kyr. Additionally, observations allow inference of the magnitude of the early Hettangian relative sea-level rise, estimated herein to have been about 55 m.

PREFACE

The current paper is the last research manuscript to which Grzegorz Pieńkowski devoted his time. Well-preserved, complete and – most of all – an almost continuous record of the uppermost Rhaetian–lower Hettangian of the Niekłań core encouraged him to gather a team of researchers from various fields of geology in order to provide a detailed stratigraphic calibration of this terrestrial succession. The preliminary results were obtained and underwent a discussion

[1] Polish Geological Institute – National Research Institute, ul. Rakowiecka 4, 00-975 Warsaw, Poland; damian.lodowski@pgi.gov.pl, marta.hodbod@pgi.gov.pl.

[2] Université de Rennes, CNRS, Géosciences Rennes, UMR 6118, F-35000 Rennes, France; mathieu.martinez@univ-rennes1.fr.

[3] Camborne School of Mines, Department of Earth and Environmental Sciences, University of Exeter, Penryn Campus, Penryn, Cornwall, TR10 9FE, UK; s.p.hesselbo@exeter.ac.uk.

[4] British Geological Survey, Keyworth, Nottingham NG12 5GG, UK; mjl@bgs.ac.uk.

amongst the group of co-authors soon before Grzegorz's passing. Now, almost two years after this heart-breaking moment, the research has been finalized so that it can be shared with scientific community.

INTRODUCTION

The Triassic/Jurassic (T/J) boundary constitutes one of the major Phanerozoic biotic turnovers, which in many respects was foundational for modern flora, fauna and the Earth system (*i.e.*, Deenen *et al.*, 2010). The end-Triassic extinction (ETE), a key element of the T/J transition, represents one of the five great mass extinction events in the Phanerozoic (besides the current one). The ETE is attributed to magmatism in the Central Atlantic Magmatic Province (CAMP) and associated outgassing of greenhouse gases, although other sources and feedbacks such as methane hydrates may also be taken into account (*e.g.*, Pálfy *et al.*, 2001; Hesselbo *et al.*, 2002). These processes resulted in long-term increase of temperature, rapid sea-level fluctuations and abrupt reduction in biological diversity (McElwain *et al.*, 1999; Pálfy *et al.*, 2001; Hesselbo *et al.*, 2002; Guex *et al.*, 2004; Marzoli *et al.*, 2004; Whiteside *et al.*, 2007, 2011; Hautmann *et al.*, 2008; Ruhl *et al.*, 2009, 2020; Schaller *et al.*, 2011, 2012; Sha *et al.*, 2011, 2015; Steinthorsdottir *et al.*, 2011; Greene *et al.*, 2012; Pieńkowski *et al.*, 2012, 2014, 2020; Heimdal *et al.*, 2020). Extensive environmental perturbations affected also the broader carbon cycle, as evidenced by a pattern of subsequent carbon isotope excursions (CIEs; *i.e.*, Korte *et al.*, 2009; Ruhl *et al.*, 2020). Ultimately, the beginning of the Jurassic was marked by a rapid marine transgressin, regarded as one of the fastest non-glacial marine inundations during the Mesozoic (Hallam, 1997).

Palaeoenvironmental conditions across the Triassic–Jurassic boundary have been studied worldwide; however, the majority of papers concern marine deposits (e.g., Pálfy *et al.*, 2001; Hesselbo *et al.*, 2002; Guex *et al.*, 2004; Marzoli *et al.*, 2004; Whiteside *et al.*, 2007; Hautmann *et al.*, 2008; Ruhl *et al.*, 2009, 2020; Greene *et al.*, 2012), while more limited data come from terrestrial successions (*e.g.*, Hesselbo *et al.*, 2002; Pieńkowski, 2004a; Sha *et al.*, 2011, 2015; Pieńkowski *et al.*, 2012, 2014, 2020; Li *et al.*, 2017). Consequently, chronostratigraphic correlation between marine and continental sections remains unlcear (Lindström, 2021; Bos *et al*., 2024); this, in turn, impairs the proper understanding of critical processes that took place during the latest Triassic–earliest Jurassic transition.

In this context, particularly important are complete and expanded terrestrial sections, which offer the possibility of cyclostratigraphic analysis. This study concerns the uppermost Triassic–basal Jurassic of the Niekłań PIG borehole, which provides an extended record of the uppermost Rhaetian–lower Hettangian developed in predominantly terrestrial clastic facies. Integration of detailed sedimentological analysis with palynology, geochemistry (stable carbon isotopes, clay mineral and elemental geochemistry analyses), and high-resolution petromagnetic investigations not only enable interpretation of the T/J environmental conditions in the Polish Basin, but also can be used for astronomical calibration of the section. Accordingly, the main aim of this research is to utilize the orbital timeframe of the Niekłań PIG core sediments in order to assess the pace of marine flooding on the continental plains of the Polish Basin during the early Hettangian ('Planorbis') transgression.

GEOLOGICAL SETTING

POLISH BASIN

During the Rhaetian–early Hettangian times, the Polish Basin (with its depocentre called the Mid-Polish Trough, MPT) was located at the northern subtropical latitude (about 40–45 degrees; Fig. 1). Running generally along the Teisseyre–Tornquist Zone (TTZ) and the Trans-European Suture Zone (TESZ), the MPT is the largest, with a length of more than 700 km. Due to its facial development (fluvial, lacustrine- to nearshore facies), definition of the T/J boundary with respect to the Hettangian GSSP (first occurrence of the ammonite *Psiloceras spelae tirolicum*; Hillebrandt *et al*., 2013) cannot be successfully applied. Consequently, the Triassic–Jurassic boundary in the Polish Basin is typically identified by palynomorphs: megaspores (Marcinkiewicz, 1962, 1971) or spores and pollen (Pieńkowski *et al.*, 2020). Insofar FO of the pollen grain *Cerebropollenites thiergartii* falls close to the base of the Jurassic (Hillebrandt *et al*., 2013), stratigraphic utility of his marker is restricted to the narrow T/J boundary interval. Consequently, studies focused on regional and supra-regional correlations exploit also other methods, such as sequence stratigraphy (Pieńkowski, 2004a; Pieńkowski *et al.*, 2020) and chemostratigraphy (stable carbon isotopes; Pieńkowski *et al.*, 2020). Noteworthy, sequence stratigraphy approach enables approximation of the Hettangian to the entire Jurassic sequence I; this, in turn, is additionally subdivided into parasequences A–K.

In the Holy Cross Mountains (HCM) segment of the Polish Basin, the Triassic–Jurassic transition accounts for stratigraphically reduced and incomplete uppermost Triassic (Zbąszynek and Parszów beds claystones, upper Norian and Rhaetian respectively) followed by more expanded and relatively complete Hettangian. The Triassic/Jurassic boundary

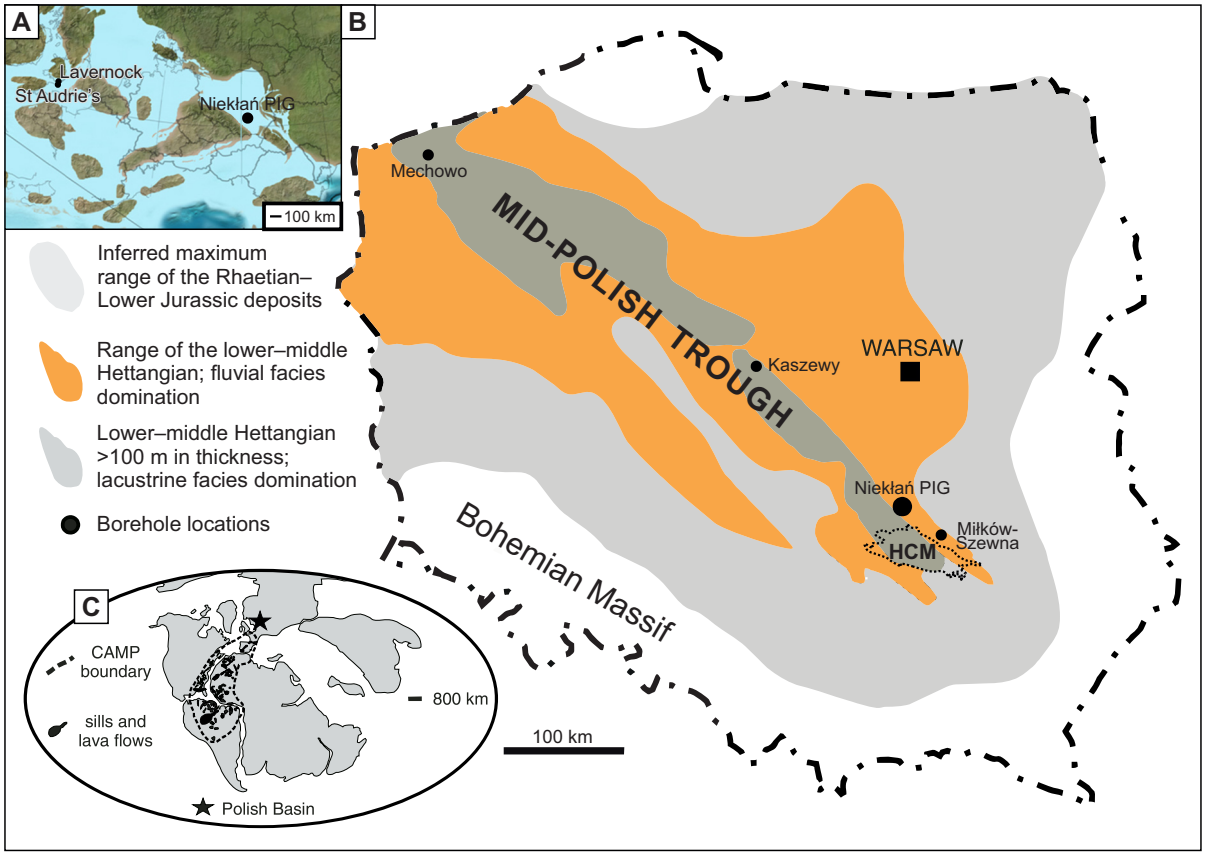

Fig. 1. Geological setting and localization of the Niekłań PIG borehole

A. Central Europe paleogeography during the Hettangian (modified after Blakey, 2020). **B.** Triassic/Jurassic transition in the Polish Basin (modified after Pieńkowski, 2004a and Pieńkowski *et al.*, 2014). **C.** Location of the Polish Basin relative to CAMP (Central Atlantic Magmatic Province)

is marked by the onset of relatively expanded sequences of claystones and sandstones of the Zagaje Fm (cf. uppermost Rhaetian–mid-Hettangian). The following, typically sandstone-dominated beds of the mid-Hettangian are included into the Skłoby Fm. Ultimately, the upper Hettangian accounts for siderite-bearing mudstones, claystones and sandstones of the Przysucha ore-bearing Fm (Pieńkowski, 2004a, 2009; Pieńkowski *et al.*, 2014).

Niekłań PIG is a 200 m deep research borehole located in the northern part of the HCM (51°09'50.00"N; 20°38'55.00"E; SE Poland; Figs. 1, 2), within the so-called Mesozoic margin of the HCM. A complete core record covering the uppermost Triassic–lowermost Jurassic beds (Brański, 2014; Pieńkowski *et al.*, 2014) enables a variety of detailed investigations, including sedimentology, bio- and chemostratigraphy, as well as astrochronology. Accordingly, the Rhaetian of the Niekłań core is thinner than in central Poland (see i.e. Kaszewy section in Pieńkowski *et al.*, 2020; Fig. 3) and contains several unconformities, whilst the Hettangian is relatively expanded. In turn, comparing to other HCM sections (*e.g.*, Huta, Miłków-Szewna; see Pieńkowski, 2004a), the Niekłań section provides relatively complete record of the Triassic–Jurassic boundary and the lowermost Hettangian (Pieńkowski *et al.*, 2014). Other T–J sections from the Polish Basin are either stratigraphically incomplete (Kamień Pomorski; Pieńkowski *et al.*, 2012) or consist of thick sandstones (Mechowo, Kaszewy; Pieńkowski 2004a; Pieńkowski *et al.*, 2020), which impairs resolution and quality of clay mineral and palynological data.

BRISTOL CHANNEL BASIN – AUXILIARY SECTIONS

The Triassic–Jurassic transition in the area of the Bristol Channel Basin (SW UK) documents a series of major-scale sedimentary turnovers, most likely related to fluctuations in relative sea level (Hallam, Wignall, 1999; Hesselbo *et al.*, 2004; Warrington *et al.*, 2008; Wignall, Bond, 2008), which manifest in lithostratigraphic division of the area. Accordingly, the Raetian interval is dominated by mudstones and

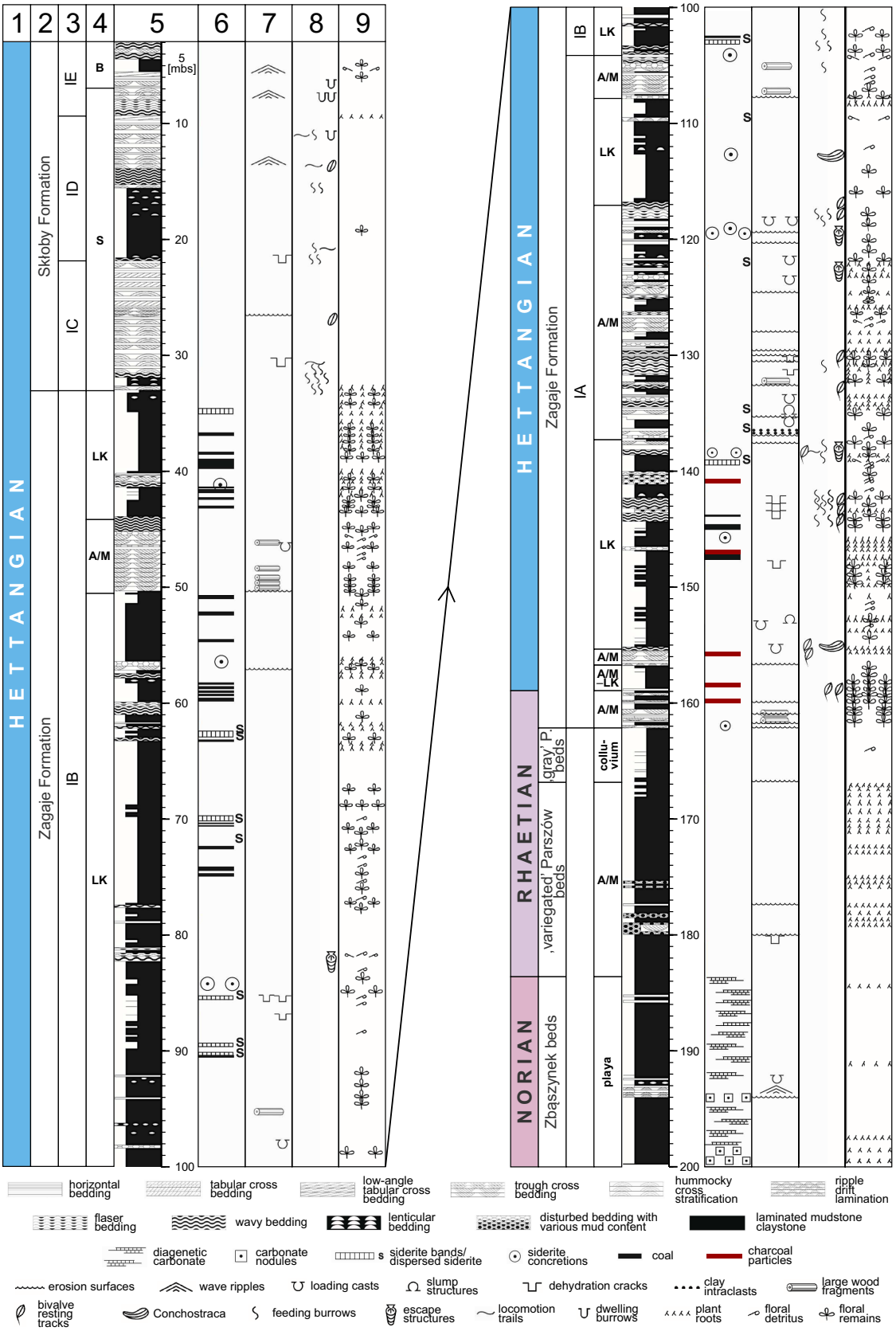
1
2
3
4
5
6
7
8
9
HETTANGIAN
Skoby Formation
Zagaje Formation
IE
ID
IC
IB
B
S
LK
A/M
LK
5 [mbs]
10
20
30
40
50
60
70
80
90
100
HETTANGIAN
RHAETIAN
NORIAN
Zagaje Formation
„variegated" Parszów beds
„gray" P. beds
Zbąszynek beds
IB
IA
LK
A/M
LK
A/M
LK
A/M
A/M–LK
A/M
collu-vium
A/M
playa
100
110
120
130
140
150
160
170
180
190
200
horizontal bedding
tabular cross bedding
low-angle tabular cross bedding
trough cross bedding
hummocky cross stratification
ripple drift lamination
flaser bedding
wavy bedding
lenticular bedding
disturbed bedding with various mud content
laminated mudstone claystone
diagenetic carbonate
carbonate nodules
siderite bands/ dispersed siderite
siderite concretions
coal
charcoal particles
erosion surfaces
wave ripples
loading casts
slump structures
dehydration cracks
clay intraclasts
large wood fragments
bivalve resting tracks
Conchostraca
feeding burrows
escape structures
locomotion trails
dwelling burrows
plant roots
floral detritus
floral remains

Fig. 2. Geological log of the Niekłań PIG core

Stratigraphy of the section based on Pieńkowski *et al.* (2014), supplemented with this study developments. 1 – chronostratigraphy; 2 – lithostratigraphy; 3 – sequence stratigraphy (parasequences); 4 – environmental interpretation; 5–8 – lithology, sedimentology and depth.
Explanations (column 4): S – nearshore and open brackish marineshelf basin; B – barrier; LK – lacustrine; A/M – anastomosing / meandering rivers

shales, (and subordinate limestones) of the Blue Anchor Fm, Westbury Fm and Lilstock Fm (with the latter being subdivided into Cotham and Langport members); these are followed by the uppermost Rhaetian–lower Jurassic limestones and mudstones of the Blue Lias Fm. This sedimentary succession, in particular the Blue Lias Fm. has been subject to wide range of bio-, chrono-, and chemostratigraphic studies (*i.e.*, Weedon *et al*. 1999, 2019; Deconinck *et al*., 2003; Hounslow *et al.*, 2004; Korte *et al.*, 2009).

This research relies on correlation with two sections located on the opposite side of the Bristol Channel: St Audrie's Bay (England) and Lavernock (Wales) (Fig. 1A). St Audrie's Bay section, a former proposal for the GSSP of the Hettangian (Warrington *et al.*, 2008), covers the Rhaetian–lower Sinemurian interval. The Hettangian is ~72 m thick and contains ammonites from Planorbis and Angulata zones (*i.e.*, Whittaker, Green, 1983). An independent astronomical calibration of the section, utilizing different methods and datasets, was provided by Ruhl *et al.* (2010; $\delta^{13}C$, $CaCO_3$, total organic carbon) and Weedon *et al*. (2019; magnetic susceptibility). The Lavernock Point section is *ca.* 45 m thick and ranges from the topmost Rhaetian up to lower part of the Angulata Zone (upper Hettangian); however, astronomical calibration is available only for the Tilmanni, Planorbis and the lower part of the Liasicus Zone (Weedon *et al*., 2019). It is worth noting, that in the UK the precise position of base of the Hettangian stage (Tilmanni Zone) is uncertain due the fact that the index taxon does not occur there and its FO is approximated via $\delta^{13}C$ stratigraphy (*i.e.*, Hillebrandt *et al.*, 2013).

MATERIALS AND METHODS

SEDIMENTOLOGY

Sedimentologic observations were performed directly on core in the geological warehouse; the entire available core was studied. Macroscopic observations were focused on lithologic changes, identification of disconformities, and recognition of different sedimentary features. Amongst the latter, special attention was paid to the type of bedding (*i.e.*, cross-beddings, hummocky cross stratification, ripple marks), occurrence of plant material and trace fossils. Collected observations were subsequently interpreted in terms of five main depositional environments: 1) playa; 2) anastomosing / meandering river; 3) lacustrine; 4) barrier facies; 5) nearshore / open brackish marine shelf. Major lithological and environmental changes were also the base for sequence stratigraphy interpretation (parasequences).

PALYNOLOGY

Palynological residues from claystones from the interval 166.7–156.8 m (17 samples) were checked for presence of palynomorphs. Standard decarbonation techniques (Halbritter *et al*., 2018) were used to remove all inorganic carbon from macrofossil plant material samples in the palynological laboratory of the Polish Geological Institute – National Research Institute (PGI-NRI). The samples were crushed to a fine homogeneous powder and then treated with two rounds of hydrochloric acid at room temperature, leaving 24 hours after the addition of hydrochloric acid; after that they were washed with deionised water and dried.

CARBON ISOTOPES

This study utilizes the organic carbon isotope record derived from wood particles ($\delta^{13}C_{WOOD}$), which is more useful than more typical $\delta^{13}C_{ORG}$ due to greater homogeneity of the analysed organic material. Fifty-eight phytoclast samples from 167–75 m interval were manually separated from kerogen at the PGI-NRI. Approximately 30–50 mg of bulk rock was crushed and then underwent two rounds of acid digestion, first using cold 30% hydrochloric acid then using 38% hydrofluoric acid. The samples were then washed with a water and hydrogen iodide solution. Cadmium iodide and potassium iodide salt solutions were used to separate out heavy minerals; subsequently the samples were washed with distilled water until neutra. Woody phytoclast particles of the same appearance (to minimise $\delta^{13}C$ variability caused by compositional changes) were hand-picked with a needle from the palynological residues, using an optical microscope. All picked woody phytoclasts from each sample were placed in a tin capsule and then analysed for carbon isotope values at the British Geological Survey Stable Isotope Facility using the Carlo Erba 1500 on-line to a VG TripleTrap (plus secondary cryogenic trap in the mass spectrometer for very low carbon content samples) and Optima dual-inlet mass spectrometer, with $\delta^{13}C$ values calculated to the VPDB scale using a within-run laboratory standard (BROC1) calibrated against NBS-19 and NBS-22. Replicate analysis of well-mixed samples indicated a precision of + <0.1‰ (1 SD).

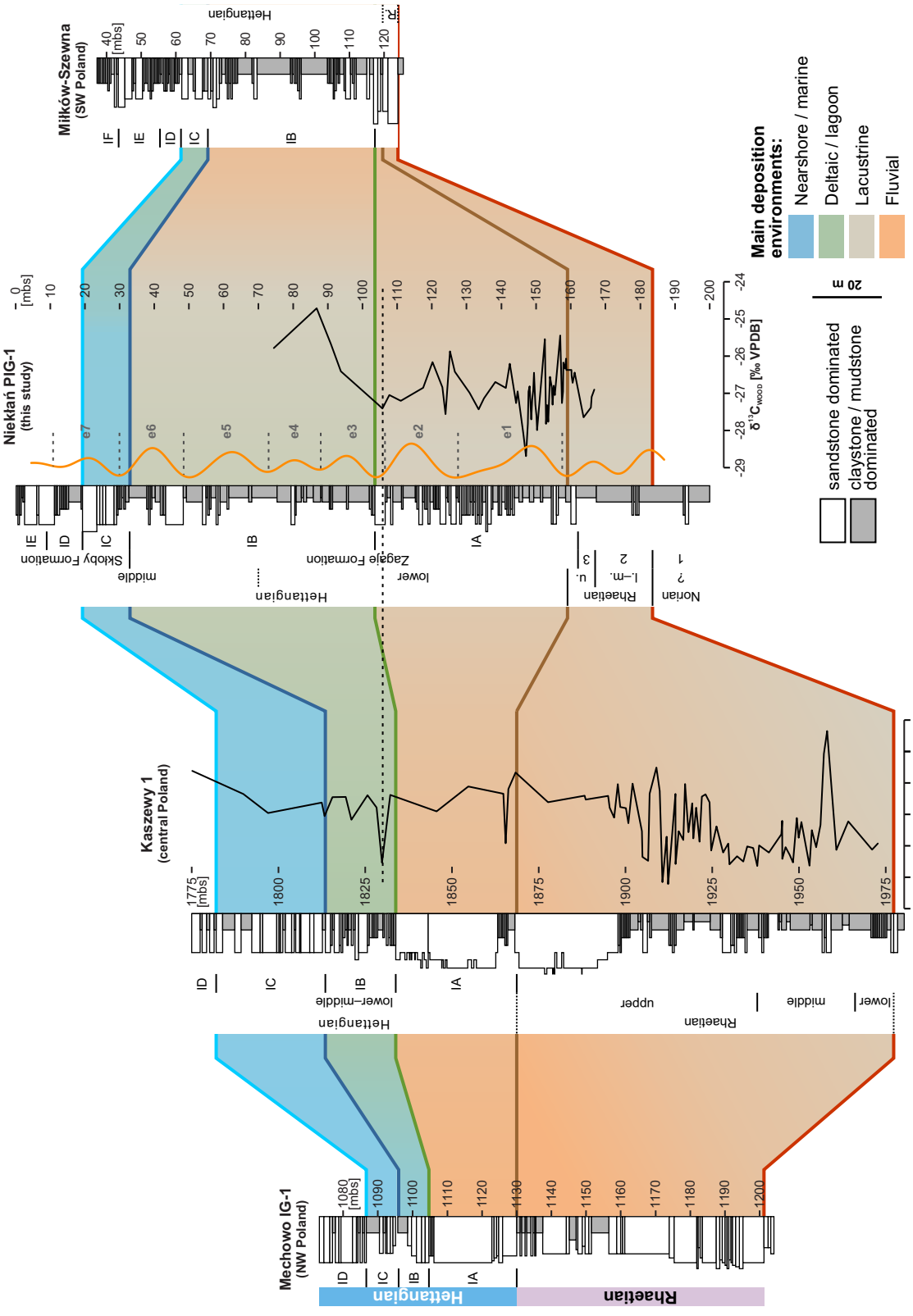

Fig. 3. Record of the early Hettangian marine transgression in the Polish Basin sections

Parasequence boundaries and stratigraphy of the Mechowo IG 1 core after Pieńkowski (1997), Kaszewy 1 after Pieńkowski *et al.* (2020), Miłków–Szewna after Pieńkowski (2004a). Different timing of parasequences IA and IB can be noted when positions of sequence boundaries are plotted against $\delta^{13}C$ curves (dashed black line). Yellow curve on Niekłań PIG 1 core indicates 100 kyr astronomical cycles documented via MS signal. Explanations and abbreviations; R. – Rhaetian; l. – lower; m. – middle; u. – upper. Thick red line indicate the base of the Rhaetian. Brown, green, dark blue and blue thick lines indicate lower limits of the successive parasequences IA–ID

CLAY MINERALS

A set of 76 samples was taken from the entire depth of the Niekłań PIG core in order to analyse the clay mineralogy; some of the results were already discussed by Brański (2014) and Pieńkowski *et al*. (2014). All samples were studied at the PGI–NRI laboratories. Each rock sample was coarsely crushed in a Fritsch crusher, dried at a temperature of 110°C, and ground to obtain a fine, homogeneous powder of the bulk rock with particles <63 μm. Bulk rock compositions and clay minerals were identified by X-ray diffraction (XRD) using a Phillips PW 3020 X'Pert diffractometer with CuK radiation. The bulk-rock mineralogy was determined on XRD patterns of powder samples. The ICDD (International Centre for Diffraction Data) database was used for qualitative determination of minerals. The Reference Intensity Ratio method, embedded in control software, was applied for semi-quantitative phase analysis. Clay minerals were identified by XRD on oriented mounts of non-calcareous clay-sized particles, separated from suspension by differential settling according to Stokes' Law. The calcareous samples were treated with 10% acetic acid for removal of carbonates. Oriented specimens were prepared by smearing a paste of the <2 micron fraction onto a glass slide. For each sample, three X-ray analyses were performed: after air-drying, ethylene-glycol solvent, and heating at 550°C. The individual clay minerals were identified using the position of the series of basal reflections on the three X-ray diagrams (Moore, Reynolds, 1997; Środoń, 2006). Kaolinite was identified using the reflection at ~7 Å, illite at ~10 Å and chlorite at ~14 Å (on the basis of X-ray diagrams of air-dried and heated specimens). Additionally, the kaolinite-chlorite doublet at 3.5 Å was used to assess the proportion of these minerals. Smectite and the rarely and locally observed illite-smectite mixed-layers (mostly with >90% illite content) were here determined on 15–17 Å and 11–13 Å peaks, respectively. Semi-quantitative estimations of clay mineral contents were based on the peak areas of basal reflections summed to 100%. SEM observations of selected samples were also performed using a LEO 1430 scanning electron microscope with an energy dispersive spectrometer (EDS Oxford Instrument).

GEOCHEMISTRY

Geochemical analyses of major elements and organic matter were performed on 34 bulk rock samples (either from claystones and sandstones) in the Chemical Laboratory of the Polish Geological Institute – National Research Institute; also in this case some data were partly published in Brański (2014) and Pieńkowski *et al.* (2014). Major elements were measured by X-ray fluorescence using a PhillipsPW 2400 spectrometer. The lower detection limits of the individual components ranged from 0.001 to 0.1% (usually 0.01%). Concentrations of several oxides (Si, Ti, Al, Fe, Mn, Mg, Ca, Na, K, P, S) were determined and recalculated to the means of their elemental content. Due to its limited diagenetic mobility, aluminum is adopted here as the main proxy for fine-grained lithogenic influx (*e.g.*, Tribovillard *et al.*, 2006). Chemical Index of Alternation (CIA) was calculated using the equation of Nesbitt and Young (1982), where CaO* is the amount of CaO incorporated in the silicate fraction of the rock, while silicate CaO is approximated to the proportion of Na_2O (*e.g.*, McLennan, 1993).

ROCK MAGNETISM

The total of 1304 volumic magnetic susceptibility (MS) measurements (with a mean step of 15 cm) were made directly on core using ZH Instruments SM30 Magnetic Susceptibility Meter. Further laboratory experiments were performed in the Paleomagnetic Laboratory of the PGI-NRI based on 70 rock samples; these were crushed into a homogenous fine-gravel fraction and packed in 8 cm^3 sample boxes.

Laboratory investigations comprised mass-normalized measurements of MS, NRM (natural remanent magnetization) and laboratory induced isothermal (IRM) and anhysteretic (ARM) remanent magnetizations. MS measurements were performed at two frequencies (976 and 15 616 Hz) using an Agico MFK1-FB Kappabridge. IRM was applied along the z-axis in a magnetic field of 100 mT ($IRM100_{mT}$) and then antiparallel in a magnetic field of 1 T (IRM_{1T}) using a Magnetic Measurements MMPM Pulse Magnetizer. ARM was produced in a Molspin ARM device with peak alternating field of 100 mT and a steady field bias of 0.1 mT. Both NRM and artificial magnetizations were measured using Agico JR6A spinner magnetometer.

The S-ratio ($-IRM_{100mT} / IRM_{1T}$) was calculated to indicate the relative proportions of low and high coercivity minerals (*e.g.*, Opdyke, Channell, 1996). A dominance of the low coercivity fraction (*e.g.*, coarse-grained magnetite) is reflected in high S-ratio values (above 0.6); as the S-ratio declines, the contribution of high coercivity minerals, for instance hematite and/or fine-grained magnetite, increases. The ARM / IRM_{1T} ratio is often used as a proxy for magnetic grain size or magnetite/hematite ratio (*e.g.*, Opdyke, Channell, 1996; Venuti *et al.*, 2007).

All the measurements are provided in a tabular form (Excel file) as an Appendix 1.

SPECTRAL ANALYSIS

Prior to the spectral analyses, the volumic MS series acquired with the SM30 (as well as literature datasets from Weedon *et al.*, 2019) was linearly interpolated to the median sampling distance, i.e. every 0.1 m in case of the Niekłań section, and 0.04 m for Lavernock and St Audrie's Bay. The long-term trend of the MS series was calculated using the LOWESS method (Cleveland, 1979) applying of coefficients of 0.5 (Niekłań, Lavernock) and 0.2 (St Audrie's Bay). In a second step, the long-term trend in variance was removed by calculating the instantaneous amplitude with a Hilbert transform, calculating the long-term trend of this instantaneous amplitude using LOWESS with a coefficient of 0.5, and divide the residual MS signal by this smoothed curve. This method of detrend ensures stationarity both in average and amplitude and ensures the spectral powers at frequencies near 0 has been sufficiently decreased without impacting or creating spurious spectral peaks at higher frequencies. Spectral analyses were made on the MS signal using the Multi-Taper Method applying three 2π tapers (Thomson, 1982, 1990). Confidence levels were calculated using the Mann and Lees (1996) robust procedure. The spectral background was calculated applying a moving median over 20% of the spectrum. Amplitude spectrograms were calculated using Time-Frequency Weighted Fast Fourier Transforms, as described in Martinez *et al.* (2015), over 50-m (Niekłań) and 8-m (Lavernock, St Audrie's Bay) width windows.

RESULTS

LITHOFACIES AND SEDIMENTOLOGY

The Niekłań section starts with red-variegated calcareous mudstones, subordinate siltstones and fine-grained sandstones, and common calcareous nodules (200.0–183.5 m; Fig. 2; Pl. 1). These strata belong to the informal regional lithostratigraphic unit called Zbąszynek beds (equivalent of Arnstadt Formation in Germany). Based on regional correlation this interval is assigned to the Norian (Marek, Pajchlowa, 1997; Wagner, 2008).

The overlying variegated reddish gray mudstones differ significantly from the Zbąszynek beds in several features: they lack carbonates, but pedogenic horizons (represented by oxidized plant roots) are common. These strata are referred as 'variegated' Parszów beds (Fig. 2; Pl. 1) – an equivalent of the lower Wielichowo beds and Exter Formation in Germany. The lower bounding surface (a significant lithologic contrast at 183.5 m depth) is regarded as a major unconformity and sedimentary hiatus; similarly, the upper boundary (167.0 m) is constituted by hiatus or unconformity.

The overlying pale gray claystones represent the 'gray' Parszów beds (167.0–162.1 m; Pls. 1, 2; equivalent of the upper Wielichowo beds or upper Triletes beds, upper Rhaetian). These homogenous strata contain no pedogenic horizons and are regarded as strongly kaolinized weathering colluvium, observed in many places in the Polish Basin (Marek, Pajchlowa, 1997).

The main subject of this paper is the superposed Zagaje Formation. The formation starts from an erosional boundary at the depth 162.1 m (Fig. 2; Pls. 2, 3) and is represented by continental coal-bearing facies (sandstones and mudstones with coals) of the uppermost Rhaetian and lower Hettangian (Pieńkowski, 2004a). Based on general lithologic appearance, the formation can be divided into two very thick parasequences (IA and IB). The lower one (162.2–104.2 m; parasequence IA) is characterized by common fluvial deposits (cross-bedded sandstones) with subordinate lacustrine facies (coal-bearing olive-gray mudstones and claystones). The lower part of the parasequence (cf. 162.1–137.5 m) is dominated by olive-gray mudstones and claystones with thin coal seams, thus it represents fluvial plain and lacustrine deposits; characteristic for its basal part (~162.1–155.0 m) are also numerous erosional surfaces and frequent charcoal particles (Fig. 2). Above (137.2–104.2 m) the most common are sandstones with characteristic fining-upward cycles (one to few meters thick) representing fluvial channels, and coarsening-upward cycles most likely representing crevasse splays. Such record points to deposition in an anastomosing and/or meandering river environments; however, lacustrine mudstones dominate also 117.2–108.1 m interval. Horizons with abundant small siderite concretions ('siderite sphaerulites') represent characteristic, early diagenetic product of pedogenic processes in permanently water-saturated soil. Shallow water tables occurring in backswamps or oxbow lakes might have created favourable conditions for deposition and preservation of plant debris, typical for the Gleysol type of palaeosol (Arndorff, 1993). Presence of bivalve burrows and conchostracans point to intermittent aquatic conditions. A multitude of coalified plant roots points to in-situ vegetation, and drifted plant fossils are also very common.

The upper parasequence (IB; 104.2–32.8 m) is clearly dominated by dark-gray-olive claystones and mudstones, locally coaly or sideritic. These laminated or massive beds are interpreted as of lacustrine origin (Fig. 2). Sandstone intercalations are rare; one significant (~ 5 m thick) bed at 50.4–45.2 m represents a fluvial channel. Few other sandy intercalations might reflect progradation of small lake deltas, as indicated by coarsening-upward cycles. Drifted plant fossils are common, but plant roots are rare, which points to perma-

nent aquatic conditions. Only the uppermost part of the parasequence (claystones at 42.4–33.0 m) show proliferation of plant roots and coal seams; in one place coal horizon is almost 1 m thick.

The topmost part of the Niekłań section (33.8–3.0 m) is constituted by pale-gray mudstones and pale-yellow sandstones of the Skłoby Formation. The formation starts with another major bounding surface represented by a sharp contact between claystone with plant roots (Zagaje/Skłoby formational boundary) and the following sandstone bed with hummocky cross-stratification (HCS). The sandstone is overlain by 1.4 m of bioturbated heteroliths and 9.8 m of cross-bedded sandstones (with HCS and tabular cross-bedding). The occurrence of relatively common locomotion trails and feeding burrows, as well as bivalve resting tracks, account for permanently aquatic conditions. In turn, scarcity of floral remains along with the occurrence of HCS suggests deposition in nearshore and/or brackish marine environment. Characteristic is also a recurring pattern of thick mudstone-sandstone couplets, what enables recognition of three parasequences: IC, ID and IE (Fig. 2).

PALYNOLOGY

Diversified spore and pollen grain assemblages (33 spore taxa and 21 pollen grain taxa plus non-discriminated saccate pollen grains) characterize the Triassic–Jurassic boundary interval (163.7–156.8m) (Fig. 2). The older beds are barren of palynomorphs, probably due to oxidizing conditions during sedimentation and early diagenesis. The colours of spores point to a low thermal alteration (Thermal Alteration Index, TAI = 2–3), typical for the Polish Basin (Pieńkowski, Waksmundzka, 2009).

The lowest two samples (161.1 and 160.7 m) contain few spore or pollen grains, except for numerous fern-derived spores *Cyathidites minor* and *Concavisporites*. Above, exceptionally abundant spores (total of 173 specimens), represented chiefly by fern-derived *Baculatisporites*, *Concavisporites*, *Cyathidites* and *Krauselisporites* (127 spores), characterize a 30 cm thick bed, at 160.3–160.0 m. This horizon is interpreted as a "fern spike" level; however, determinable pollen grains are few, with most destroyed, corroded and most probably redeposited.

Higher in the section (158.9 m) an important palynological turnover is observed. The assemblage becomes rich in *Aratrisporites minimus* (lycopod microspore) and *Pinuspollenites minimus* (Pinaceae-Podocarpaceae pollen grain). Mass occurrence of the pollen grain *Classopollis* sp. (Cheirolepidiaceae) is also characteristic of this turnover. Moreover, slightly above, at 158 m, there is the first occurrence (FO) of the pollen grain *Cerebropollenites thiergartii* Schulz 1967. A second level dominated by spores (82 spores, mostly *Concavisporites* and *Cyathidites* minor) is documented at the depth 156.8 m; pollen grains are almost absent. This level is interpreted as a second "fern spike".

Above, the palynomorph assemblage is rather uniform, with sixty-three taxa of spores and pollen grains typical for the Jurassic, including pollen grains: *Classopollis*, *Pinuspollenites*, *Vitreisporites*, *Monosulcites*, *Chasmatosporites*, *Perinopollenites*, and spores *Aratrisporites minimus* and *Concavisporites* (Ziaja, 2006).

ORGANIC CARBON ISOTOPES

The record begins with strongly negative values (–26.9 to –27.7‰ VPDB) in the upper Rhaetian (166.0–163.5 m). The Rhaetian/Hettangian boundary interval (161.0–157.5 m) is marked by elevated $\delta^{13}C_{WOOD}$ (*ca.* –26.5 ‰ VPDB). Above (157.5–148.0 m) the section accounts for generally decreasing, yet bed-by-bed variable isotopic signatures, starting with a maximum of –25.4 ‰, pronounced peak (–25.6 ‰ VPDB) at 153.4 m, and a minimum of –28.7 ‰ VPDB at 148 m. Ultimately, an increasing $\delta^{13}C_{WOOD}$ trend, up to –26.2 ‰ VPDB, occurs over the 148.0–143.3 m interval. The overlying beds have lower sampling resolution, but two local peaks can be observed at 126.1 and 87.6 m (–25.8 and –24.7 ‰ VPDB, respectively) (Fig. 4).

CLAY MINERALOGY

The base of the section (200.0–183.5 m: Zbąszynek beds, Norian) is characterized by preponderance of smectite, with subordinate content of kaolinite and chlorite (Fig. 4). In contrast, the following 'variegated' Parszów beds (= lower Wielichowo beds, lower–middle Rhaetian; 183.5–167.0 m) are characterized by the domination of kaolinite and fair illite admixture. The successive 'gray' Parszów beds (= upper Wielichowo beds, middle–upper Rhaetian; 167.0–162.1 m) accounts for maximum share of kaolinite-and associated illite admixture (Fig. 4).

Ultimately, the Zagaje Formation (162.1–33.8 m, uppermost Rhaetian–lower Hettangian) is characterized by kaolinite-smectite-chlorite association, with fluctuating kaolinite and smectite content and generally decreasing chlorite. In the lowermost part of the Zagaje Fm (162.1–150.0 m) smectite is relatively less abundant, while kaolinite and chlorite contents are relatively slightly higher. Kaolinite diminishes gradually from 162.1 to a depth of c. 145 m and then rises again between 145 and 108.5 m. Above 108.5 m kaolinite content is generally stable (Fig. 4). Ultimately, the top of the section (Skłoby Formation; 33.0–3.0 m) depicts

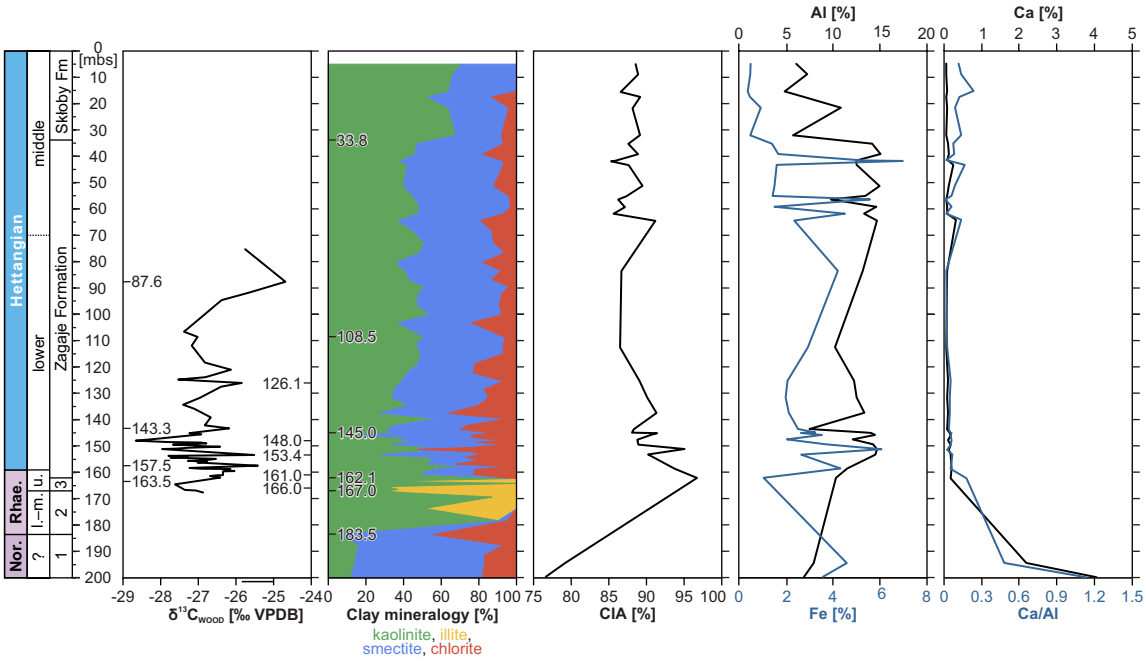

Fig. 4. $\delta^{13}C_{WOOD}$, clay mineralogy, and CIA, as well as Al and Fe concentrations in the Norian–Hettangian of the Niekłań PIG core

Explanations: 1 – Zbąszynek beds; 2 – 'variegated' Parszów beds; 3 – 'gray' Parszów beds. Abbreviations: Nor. – Norian; Rhae. – Rhaetian; l. – lower; m. – middle; u. – upper

slightly elevated share of kaolinite, relative to the underlying strata.

ELEMENTAL GEOCHEMISTRY

An upwards decrease in calcium (Ca) content, from 4% to ~0.1–0.2%, is observed in Niekłań core between 200 and 160 m; above, up to the top of the section, Ca content remains usually below 0.1% (Fig. 4). Aluminum (Al), in turn, shows an increase from ~7% to almost 15% from the base of the core (200 m) up to 150 m. Contributions ranging between 10–15% are characteristic of 150–35 m interval, whilst the topmost part of the core manifests decreasing trend of Al content (Fig. 4). Similar observations apply to the Fe curve but without a clear initial increase in the lowermost part of the section (Fig. 4). The characteristics for the Ca/Al curve are: 1) a significant decrease at the base of the section, from >1 to near-zero (200–150 m; Norian–basal Hettangian); and 2) slightly elevated (an increasing) values within the upper part of the section (above 75 m; Appendix 1).

The minimum CIA values (< 80%) are observed within the Norian part of the section (200–190 m; Fig. 4). Above, data are available only for the Rhaetian/Hettangian transition interval. There, the uppermost Rhaetian beds manifest extraordinary high CIA (97%, 162.2 m), which progressively declines up in the Hettangian, to 86% at 112.5 m. Similar values (85–90%) are observed also in the upper part of the section (above 100 m; Fig. 4).

ROCK MAGNETISM

Comparison of laboratory (Fig. 5) and field-measured MS (Fig. 6A) allowed compilation of a reliable high-resolution curve with noticeable cyclicity. Laboratory data does not reveal any clear MS trends, except generally decreasing MS through the Hettangian, in particular its upper part (uppermost Zagaje–Skłoby Fm), from the mean of ca. 1×10^{-7} m^3/kg at 150 m, to ca. 0.25×10^{-7} m^3/kg at the top of the core. When consider high-resolution field MS, one may notice variable (apparently cyclic) and relatively elevated (mean ca. 0.2×10^{-3} SI) MS of the 200–50 m interval, followed by a decreasing values above (uppermost Zagaje–Skłoby Fm). Predominantly low values (0–0.2×10^{-6} Am^2/kg) throughout almost the entire log are characteristic of NRM; only the basal part of the section (below 165 m) accounts for single extraordinary high measurements (Fig. 5). Both IRM_{1T} and IRM_{100mT} remain stable through most of the core; however, an important increase in IRM_{1T} (from ~0.2 up to 1.9×10^{-3} Am^2/kg) is observed below 165 m.

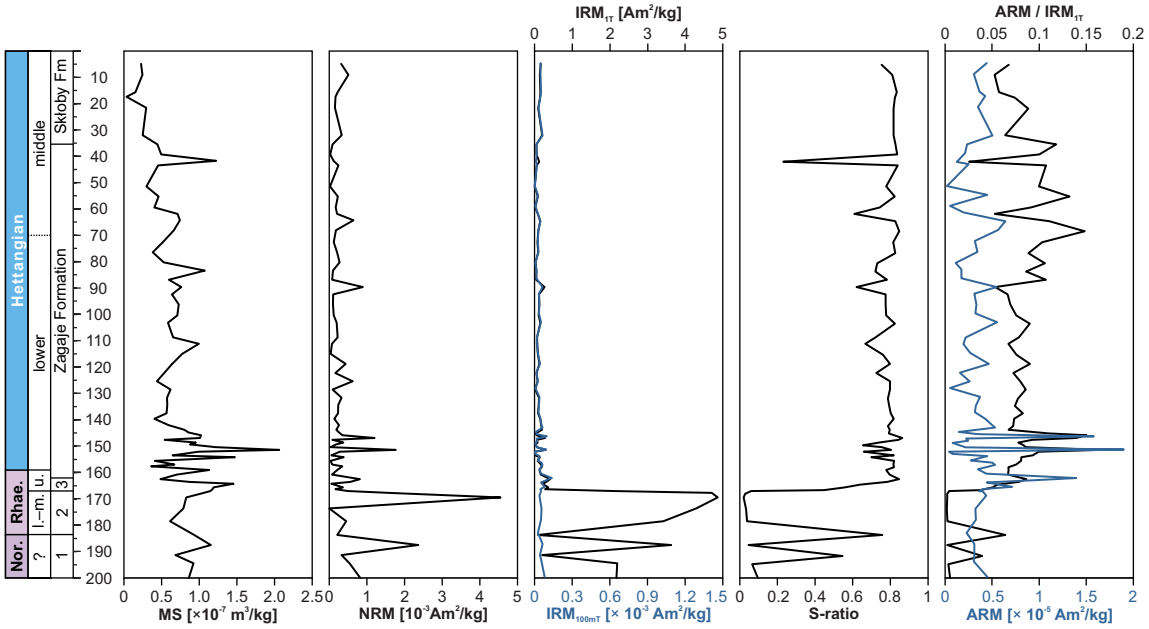

Fig. 5. Petromagnetic properties of the Norian–Hettangian of the Niekłań section

Explanations and abbreviations as on Figure 4

Also, ARM remains relatively low and stable through most of the log (usually below 0.5 × 10^{-5} Am^2/kg); minor peaks are observed only within the 170–140 m interval (Fig. 5).

The entire 165–3 m interval shows S-ratio values of ~0.75–0.80 (single point with decrease to below 0.3 occurs at 41.8 m). Below, the S-ratio significantly decreases to as low as below 0.1, however single horizons with higher values are also observed (Fig. 5). To some extent, the ARM/IRM_{1T} curve is similar – elevated values characterize the 165–3 m interval, whereas in the lowermost part of the core the ratio is significantly lowered. Besides, higher values in the ARM/IRM_{1T} are noted between 90 and 80 m, whilst a decreasing trend is observed above (Fig. 5).

Very good correlation between the Fe content and MS (Pearson correlation coefficient, r = 0.90) allow the inference that magnetic minerals are the main carrier of Fe. Furthermore, similar trends are observed also in both Fe and Al, except the lowermost interval (200–160 m; Fig. 4); this suggests predominantly detrital origins of magnetic minerals. This interpretation gains reliability considering that neither Al nor MS vary significantly within the 160–50 m interval and that they both show decreasing trends above (compare Figs. 4, 5). Nevertheless, it should be noted, that the statement above is not clearly supported by statistics ($R_{MS/Al}$ = 0.54); this is thought to result from relatively low – in comparison to MS data – coverage of the Niekłań IG 1 core by geochemical datapoints.

SPECTRAL ANALYSIS

Niekłań

The 2π-MTM spectrum of the MS series acquired with the SM-30 shows prominent cycles at 22 m and 10 m, largely exceeding the 99% confidence level (CL) (Fig. 6C). Other cycles exceeding the 99% CL are observed at 8.1, 6.3, 4.3, 3.3 and 2.1 m. The amplitude spectrogram of the series shows that the 22-m band is continuous throughout the studied interval. The record of this band starts in the Rhaetian in which the spectrogram shows several modes at various frequencies (Fig. 6D). This can be related to the multiple hiati recorded in the sedimentary pattern (see section Lithofacies And Sedimentology; see also Meyers, Sageman, 2004). The band then show periods around 30 m between depth 160 to 130 m before decreasing to ~20 m from 100 m depth upwards. Other peaks have more scattered expression. The 10-m peak is expressed with high amplitudes around 110 m and near the top of the series. The 8-m peak is expressed in the Rhaetian only, and possibly corresponds to the local expression of the 10-m peak in an interval showing reduced sedimentation rates compared to the base of the Hettangian. The 6-m peak is expressed near a depth of 50 m, the 4.3-m peak has locally high amplitudes in the Rhaetian, and around depths of 120 and 60 m. The 3.3-m peak is evident from 160 to 110 m depths.

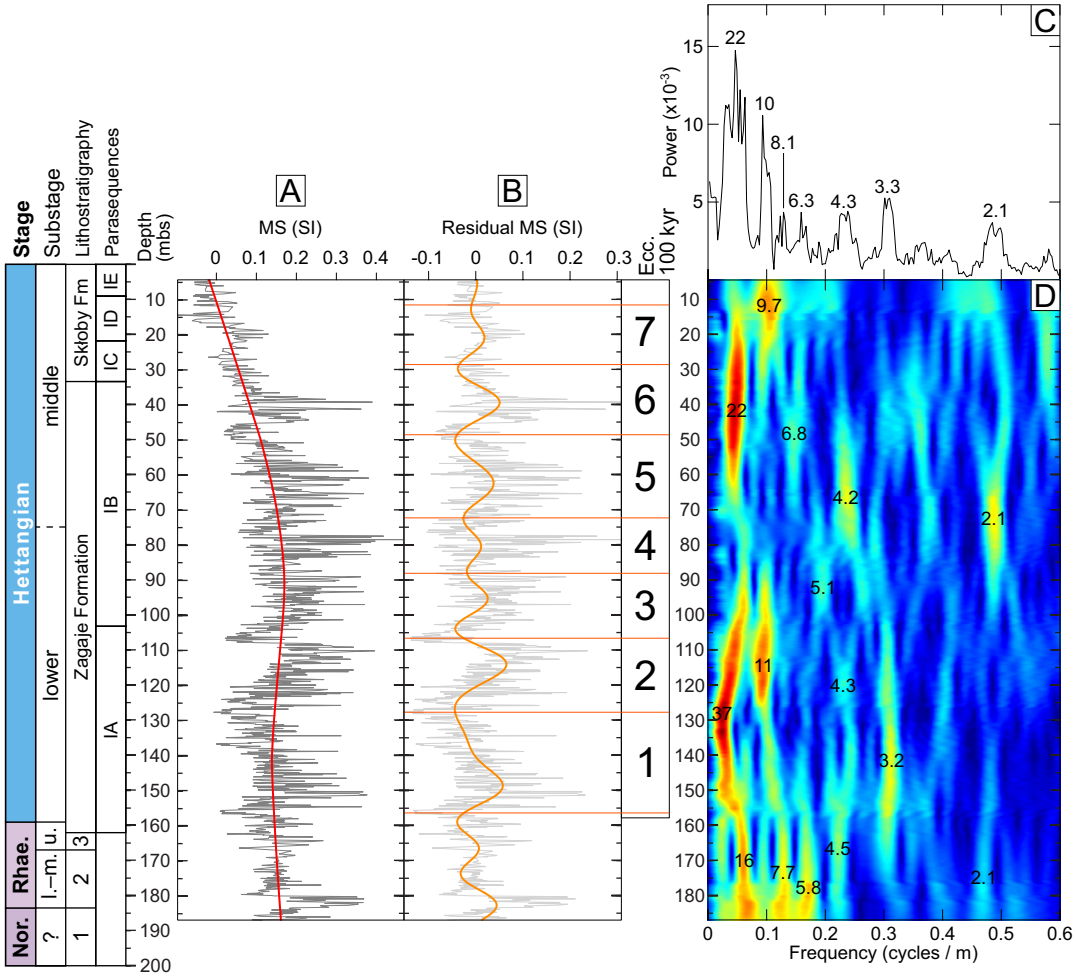

Fig. 6. Astronomical calibration of the Niekłań section

A. Raw MS signal (gray) and a long-term trend (0.5 LOWESS; thick red line). **B.** Residual (detrended) MS (light gray) and filtered 100 kyr cycles (orange). **C.** The results of Multi-Taper spectral analysis. **D.** Fast-Fourier Transforms amplitude spectrogram. Explanations and abbreviations as on Figure 4

The peak of 2.1 m is visible from depth 90 to 60 m. The peak of ~20 m is the only one that has stratigraphic continuity throughout the series.

Lavernock and St Audrie's Bay (UK) – a reassessment

In order to provide a precise astrochronologic calibration of the Hettangian of the Niekłań section, this study relies on correlation with high-resolution MS data from Lavernock and St Audrie's Bay (SW UK; Weedon *et al.*, 2019). However, as the age model adopted by the authors remains questionable, this research attempts to reassess the cyclostratigraphic interpretation of the lower Hettangian interval of those localities.

In case of the Lavernock section, the spectral analyses show two main spectral peaks at 4 and 0.8 m, attributed to the 100-kyr eccentricity cycle and the precession cycle respectively (Fig. 7D). In the amplitude spectrogram, both cycles are continuously recorded. The 4-m cycle has nonetheless periods ranging from 3.2 m at level 6 m to 5.7 m at level 15 m (Fig. 7C).

The spectrum from first 28 m of the MS record of St Audrie's Bay shows a peak of 3.1 m and another peak of high amplitude at 0.94 m (Fig. 7H). On the amplitude spectrogram, the cycle of 3.1 m shows periods around 4 m from the base of the series to level 8 m, and then decreases to ~2.5 m up to the top of the studied interval (Fig. 7I). Furthermore, also the peak of 0.94 m is found throughout the series.

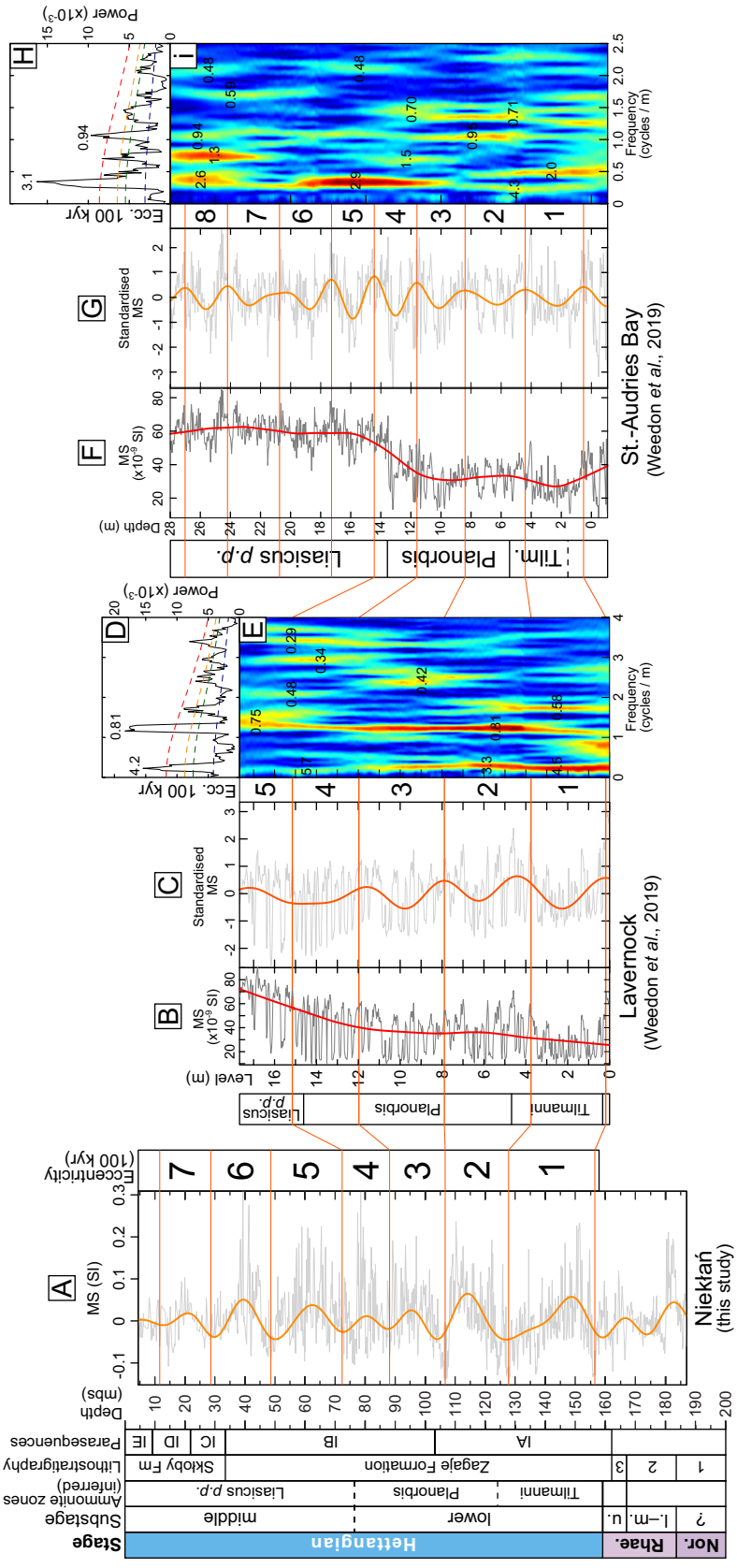

Fig. 7. Correlation of inferred astronomical cycles between the Niekłań PIG core (A; this study), Lavernock (B–E; Weedon *et al.*, 2019) and St-Audrie's Bay (F–I; Weedon *et al.*, 2019)

A. The record of 100 kyr eccentricity cycles in the Niekłań Core (as on Fig. 5). **B.** MS (gray) and a long-term trend (thick red line) reevaluated for the Lavernock site. **C.** Detrended MS (light gray) and filtered 100 kyr cycles (orange) in the Lavernock. **D.** The results of Multi-Taper spectral analysis in the Lavernock. **E.** Fast-Fourier Transforms amplitude spectrogram for the Lavernock site. **F.** MS (gray) and a long-term trend (thick red line) reevaluated for the St Audrie's Bay. **G.** Detrended MS (light gray) and filtered 100 kyr cycles (orange) in the St Audrie's Bay. **H.** The results of Multi-Taper spectral analysis in the St-Audries Bay. **I.** Fast-Fourier Transforms amplitude spectrogram for the St Audrie's Bay.
Explanations and abbreviations as on Figure 4

INTERPRETATION AND DISCUSSION

STRATIGRAPHY OF THE NIEKŁAŃ SECTION

Palynostratigraphy

A characteristic feature of the Rhaetian–Hettangian transition in the Niekłań core is mass occurrence of the pollen grain *Classopollis* sp. (Cheirolepidiaceae) at the 158.9 m level (second "fern spike"). In the Holy Cross Mountains, a proliferation of Cheirolepidiaceae is indicated by the common occurrences of shoots as well as male and female cones of *Hirmeriella muensteri* conifer, with *Classopollis* found *in situ* in the male cones of *Hirmeriella muensteri* (Reymanówna, 1992; Ziaja, 2006; Barbacka *et al.*, 2010). These trees formed forest canopy and represent a common element of the earliest Hettangian floral assemblage, known from the Sołtyków outcrop located 4 km SW from Niekłań (Pieńkowski, 2004b), which approximately corresponds to the 157–140 m depth interval of the Niekłań section (Pieńkowski *et al.*, 2014). In Sołtyków the bennettitalean *Pterophyllum alinae* also occurs, the other element of the Hettangian floral assemblage (Barbacka *et al*., 2010). Ultimately, a widespread proliferation of Cheirolepidiacean conifers and high abundances of *Classopollis* are known in the lowermost Jurassic successions worldwide (Olsen *et al.*, 2002; Whiteside *et al.*, 2007; Gotz *et al.*, 2009; Larsson, 2009; van de Schootbrugge *et al.*, 2009; Bonis *et al.*, 2009, 2010; Pieńkowski *et al.*, 2012; Vajda *et al.*, 2013; Li *et al.*, 2017).

Furthermore, the Rhaetian–Hettangian boundary in the Niekłań core can be successfully approximated with the FO of *Cerebropollenites thiergartii* Schulz (1967), the only post-Triassic miospore with its first occurrence close to the base of the Jurassic (Hillebrandt *et al.*, 2013; Gravendyck *et al*., 2023). Noteworthy, the lower part of the Sołtyków section is characterized by the occurrence of conchostracans *Bulbilimnadia kilianorum*, which points to the earliest Hettangian age (Niedźwiedzki, 2011; see also Weems, Lucas, 2015).

Altogether, the position of the Triassic–Jurassic boundary in Niekłań is well-constrained in terms of palynostratigraphy, being additionally supported by conchostracan findings.

Carbon isotope stratigraphy

Carbon-isotope excursions are important for chemostratigraphic correlation between biostratigraphically-constrained marine deposits and terrestrial sediments, where biostratigraphic constraints (mainly palynomorphs) are of poorer resolution (Pieńkowski *et al.*, 2020). A sharp negative carbon-isotope excursion (CIE), named 'initial' CIE (Hesselbo *et al.*, 2002) located just below the Triassic–Jurassic boundary was first reported by Ward *et al.* (2001); it has been interpreted to have resulted from CO_2 outgassing associated with the CAMP, or gas hydrate release (Hesselbo *et al.*, 2000, 2002, 2007; Pálfy *et al.*, 2001; Beerling, Berner, 2002; Ruhl, Kürschner, 2011; Ruhl *et al.*, 2020) in a similar manner to the later and much broader early Hettangian negative CIE (often referred to as the 'main' CIE). The 'initial' CIE coincided with both the onset of volcanic activity in the CAMP area, and floral and faunal turnovers on land and in the ocean (Hesselbo *et al.*, 2002). Fox *et al.* (2021) cast some doubt on the global significance of the 'initial' CIE and attributed its origin to the C-isotope fractionation associated with a local organic matter source, related to regional sea-level change. However, this CIE is recorded in other sections worldwide, both in marine (Ruhl *et al.*, 2020) and in continental deposits (Hesselbo *et al.*, 2002; Whiteside *et al.*, 2011; Pieńkowski *et al.*, 2020), which strongly suggests that this CIE reflects a real global carbon cycle disturbance. The two negative excursions are separated by a positive excursion, within which there is a secondary negative CIE (e.g. in St Audrie's Bay, Southern UK, Korte *et al.*, 2009; Prees 2C core, central UK, Hesselbo *et al*., 2023; Ruhl, Kürschner, 2011; the New York Canyon, Bartolini *et al*., 2012; or in the Neuquén Basin, Ruhl *et al.*, 2020; see also Fig. 8), that coincides with the first occurrence of the oldest Jurassic ammonites, *Psiloceras spelae* and *Psiloceras tilmanni*, concomitant with the beginning of the ammonite recovery, and defining the beginning of the Jurassic (Hillebrandt *et al.*, 2013).

Unfortunately, the upper Rhaetian of the Niekłań not only lacks a high-resolution isotopic data, but also is not complete due to a hiatus at the transition from 'gray' Parszów beds to the Zagaje Fm (Fig. 2). Due to that, a negative peak in $\delta^{13}C_{WOOD}$ at 164–163 m can be correlated either with the 'initial' CIE (uppermost Rhaetian) or the preceding 'precursor' CIE (Fig. 8). Nevertheless, the base of the Zagaje Fm. is characterized by elevated isotopic signatures (162–159 m), characteristic of the Rhaetian/Hettangian boundary all over the world (Fig. 8); that being said the base of the Hettangian in the Niekłań core is placed at 159 m, slightly below the FO of *C. thiergartii* (158 m). Consequently, a stepwise decrease in carbon isotopic signatures observed above, around 150 m, is thought to correspond to the onset of the 'main' CIE. Characteristic are also slightly elevated and variable $\delta^{13}C_{WOOD}$ at 130–120 m; these are correlated with variable $\delta^{13}C_{ORG}$ in the lower part of the Planorbis Zone of Prees 2C core (Fig. 8; Hesselbo *et al*., 2023) and St Audrie's Bay (Hesselbo *et al*., 2002; Ruhl *et al*., 2010). Ultimately, relatively high (highest in the entire dataset) isotopic signatures around 85 m are thought to reflect a mid-Planorbis positive excursion of the Prees 2C core

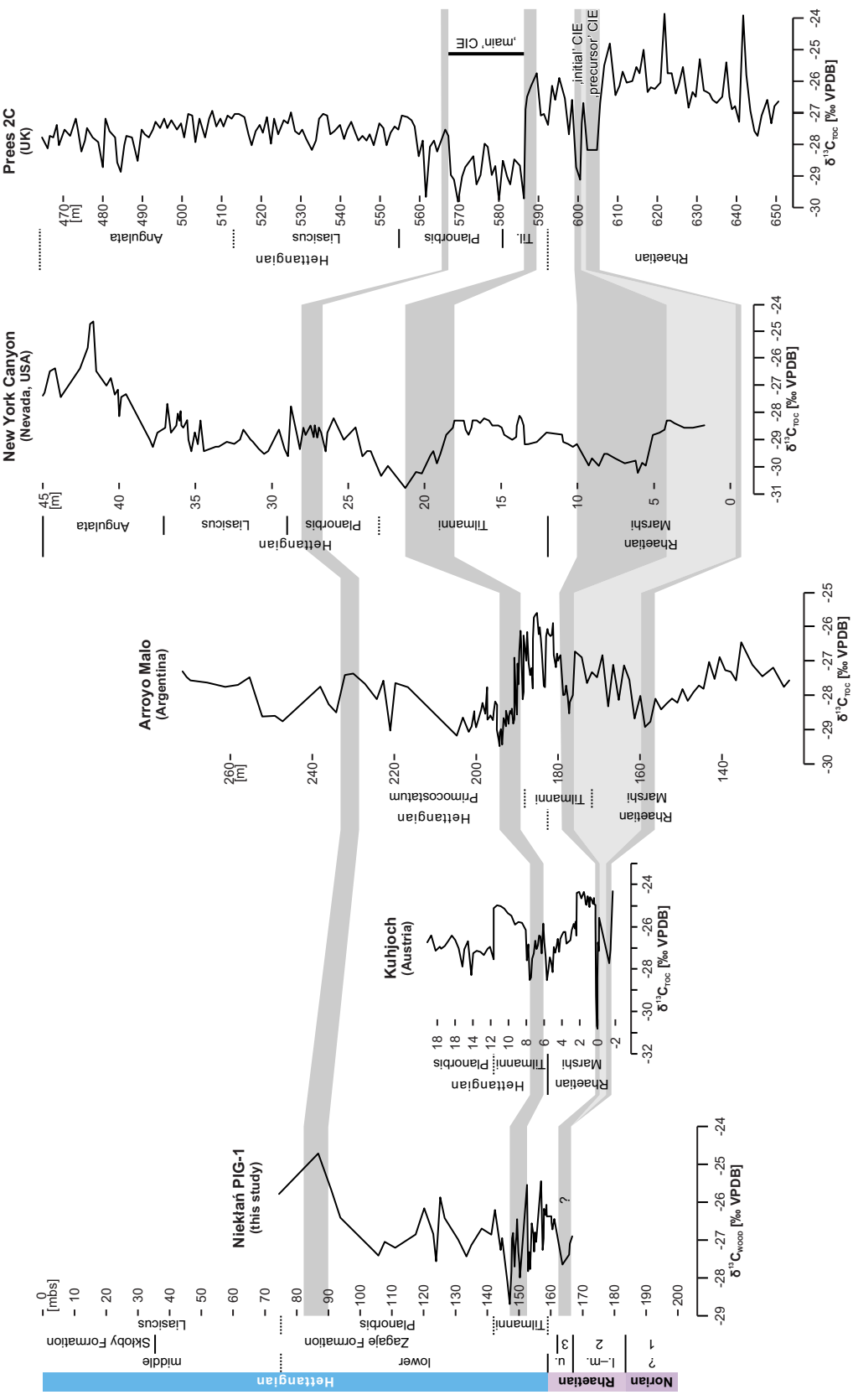

Fig. 8. Correlation of stable organic carbon isotopes ($\delta^{13}C_{ORG}$) between Niekłań PIG 1 core (this study) and Kuhjoch GSSP section (Ruhl *et al.*, 2009), Arroyo Malo (Ruhl *et al.*, 2020), New York Canyon (Bartolini *et al.*, 2012) and Prees 2C core (Hesselbo *et al.*, 2023)

Note the uncertain dating of the uppermost Rhaetian ('precursor' CIE) in the Niekłań borehole. Abbreviations and explanations: l.–m. – lower–middle; u. – upper; 1 – Zbąszynek beds; 2 – 'variegated' Parszów beds; 3 – 'gray' Parszów beds. Ammonite zonation in the Niekłań section is approximated based on carbon isotope- and cyclostratigraphy

(Fig. 8) and St Audrie's Bay section (see also Ruhl *et al*., 2010).

Astronomical calibration

Combination of detailed $\delta^{13}C$ record of the Rhaetian/Hettangian boundary interval along with periodicity observed in the high-resolution MS data from the Niekłań core can be used for stratigraphic calibration of the Hettangian of the Polish Basin.

In this context, recent years have brought an intense debate on the issue of duration of the Hettangian, ranging from <2 up to >4 Myr (see Storm *et al*., 2020 and references therein). The lowermost Hettangian Tilmanni Zone was estimated to cover ~150 kyr according to Ruhl *et al.* (2010) and *ca.* 0.5 Myr based on Weedon *et al.* (2019); similarly, the following Planorbis Zone was estimated as ~250 kyr (Ruhl *et al.*, 2010) and 1.2 Myr (Weedon *et al*., *op. cit.*). Recent calibration of the Sinemurian and Pliensbachian stages (Ruhl *et al*., 2016; Leu *et al*., 2024) together with radiometric ages available near the Triassic–Jurassic boundary and the Hettangian–Sinemurian boundary (Schaltegger *et al*., 2008; Schoene *et al*., 2010) rather point to a short duration of the Hettangian Stage.

Correlating the $\delta^{13}C_{WOOD}$ of the Niekłań core to other records dated with ammonite biostratigraphy (Fig. 8) suggest that the minimum in the $\delta^{13}C_{WOOD}$ curve at 147 m depth in Niekłań core corresponds stratigraphically with the Tilmanni Zone, while the maximum in the $\delta^{13}C_{WOOD}$ curve at 87 m depth is equivalent to the upper part of the Planorbis Zone. This interval represents approximately 250 kyr from the astrochronology of Ruhl *et al*. (2010). The same interval in Niekłań core encompasses approximately 2.5 repetitions of ~20 m cycles, which would then correspond to the 100-kyr eccentricity cycle.

However, precise correlation with St Audrie's Bay section of Ruhl *et al*. (2010) is hampered due to relatively low resolution of the data from the lower Hettangian interval. Consequently, this research reassess the high-resolution MS data (measured at even distance of 0.04 m) from the Lavernock and St Audrie's Bay (both SW UK) of Weedon *et al*. (2019) in order to fit them to short-Hettangian age model (Fig. 7).

In British sections, alike in Niekłań, the first cycle is bounded at the base of the Hettangian, therefore the maxima of the filter of the 100-kyr cycles are used to sequence the series. By extrapolating and correlating theses cycles to the Niekłań core, the Tilmanni and Planorbis zones should be approximated to the lower ~80 m of the Zagaje Fm of the Niekłań core (~77–159 m; Fig. 7A). In the Polish Basin the Planorbis/Liasicus boundary is typically correlated with transgressive system tract of parasequences IC–F (Pieńkowski, 2004a; Barth *et al.*, 2018); in case of the Niekłań PIG core this is the base of the Skłoby Fm (33 m). However, the above correlations indicate that the Tilmanni/Planorbis zonal boundary should be placed within the upper part of parasequence IA (~125 m), while the Planorbis/Liasicus boundary is located in mid part of parasequence IB (~77 m).

PALEOENVIRONMENTAL INTERPRETATION

Biotic response for the end-Triassic extinction

The Niekłań core shows evidence for two fern spikes, one marking the uppermost Rhaetian and the other already within the basal Hettangian. Such a record corresponds not only with the Pomeranian succession of the Polish Basin (NW Poland; Pieńkowski *et al*., 2012, 2014), but also with phenomena documented in other parts of the world (Deenen *et al*., 2010; Whiteside *et al*., 2011; Blackburn *et al*., 2013). Occurrence of ferns and lack or scarcity of pollen produced by Cheirolepidiaceae point to significant vegetation crises, most likely connected with volcanic volatiles, acid rain, soil loss, defoliation and possibly transient cooling (Ganino, Arndt, 2009, van de Schootbrugge *et al*., 2009, 2020; Schaller *et al*., 2012; Bos *et al.*, 2024). These crises may indicate end-Triassic extinction, which possibly took place in more than one phase (Pieńkowski *et al*., 2014; Wignall, Atkinson, 2020; Lindström, 2021).

Paleoclimate conditions

Clay mineral and geochemical (CIA) data collected for this study allow interpretation of the paleoclimate conditions prevailing the area of the Polish Basin during the Triassic–Jurassic transition (see also Brański, 2014; Pieńkowski *et al.*, 2014). Abundant smectite and low kaolinite, together with low CIA (Fig. 4), suggest hot dry to semi-dry seasonal palaeoclimate for the Norian–earliest Rhaetian (playa-type deposits; 200.0–183.5 m), typical for this part of Europe (Feist-Burkhardt *et al*., 2008; Preto *et al.*, 2010; Brański, 2014). Later on, the early–middle Rhaetian brought seasonal and gradually more humid conditions, as manifested by a kaolinite-illite association with general domination of kaolinite and numerous pedogenic horizons (183.5–167.0 m). Dominance of kaolinite (up to 100%) and maximum CIA values within the 167.0–162.1 m indicate intense hydrolysis under the warm and humid climate of the late Rhaetian; importantly, similar conditions were documented along the eastern margin of the Central European Basin (Ahlberg *et al*., 2003). The climate changed along with the Rhaetian/Hettangian

(T–J) transition, when transient cooling (see above) was followed by climate aridization, as evidenced by lowered share of kaolinite (to below 40% at 150–125 m), decreasing CIA, and frequent charcoal particles (= wildfires; 162.1–155.0 m). Nonetheless, the later stages of the Hettangian were most likely milder, as evidenced by slightly higher kaolinite content (40–50%) and the lack of wildfire indicators. Ultimately, elevated kaolinite within 33–3 m interval (Skłoby Formation) is interpreted as a result of epigenetic weathering, which occurred after inversion of the Mid-Polish Trough during the ?latest Cretaceous–Paleogene (Brański, 2006).

EARLY HETTANGIAN MARINE TRANSGRESSION IN THE POLISH BASIN

Timing and duration of the 'Planorbis' transgression

Rapid sea-level rise during the Planorbis Zone was inferred already by Bloos (1976), who noted that in Bavaria the Rhaetian strata are cut and overlain by fluviatile lowermost Hettangian and the following marine shales of Planorbis Zone. This case resembles the situation in the Polish Basin, where early Hettangian transgression and sedimentation was preceded by erosion of Rhaetian deposits connected with late Rhaetian lowstand (Pieńkowski, 2004a; see also Hallam, 1997, 2001; Coe, Hesselbo, 2000; Haq, 2017, 2018).

Accordingly, the first major sedimentary turnover within the Hettangian at Niekłań is observed at 104 m, where fluvial deposits are replaced by typically lacustrine facies (parasequence IA/IB boundary, Zagaje Fm; Fig. 2). This phenomenon is well-known also from other HCM sections, where it is associated with a fast rise of base-level during the Planorbis marine transgression (Pieńkowski, 2004a). Later on, progressive increase of base-level led to marine flooding, as manifested by the onset of nearshore/marine facies at the base of the Skłoby Fm (33 m; Fig. 2) and increase in Ca content (Fig. 4), as well as lowered ARM/IRM_{1T} (Fig. 5), most likely reflecting fining of grain size (*i.e.*, Opdyke, Channell, 1996; Jovane *et al.*, 2007; Venuti *et al.*, 2007). When considering astrochronologic calibration, parasequence IA covers the e1–e2 cycles and the basal half of e3 cycle, ~200 kyr in total; in turn, parasequence IB correlates with the upper part of e3 cycle, e4–e5 cycles and the lower part of e6 cycle, or a total of ~350 kyr (Fig. 6). Here it should be also noted, that even though terrestrial (predominantly fluvial and lacustrine) facies of the Niekłań section account for common stratigraphic gaps, cyclostratigraphic (Fig. 7) and $\delta^{13}C$ (Fig. 8) correlations allow to infer that none 100-kyr cycles was removed from the record. Nevertheless, some significant contrasts in MS signal (i.e. around 120–115 m or 80–75 m; Fig. 6) are most likely associated with the occurrence of erosional gaps, as evidenced also by sedimentologic observations (Fig. 2).

Astrochronological constraints and carbon isotope correlation between Poland (this study) and the UK (Figs. 7, 8) allow an estimate of the timing of marine encroachment through the Polish Basin, from North-Western Poland (Pomerania), through central Poland (Kaszewy), and to the HCM (Fig. 3). In NW Poland (Mechowo IG 1 borehole; Pieńkowski, 1991, 2004a) the first deposits which can be attributed as 'marine' are found at the base of parasequence IB (Fig. 3; Pieńkowski, 2004a). According to estimated time covered by the parasequence IA in Niekłań, the marine flooding in NW Poland post-dated the beginning of the Jurassic by ~200 kyr and the marine transgression in SW UK for some ~300 kyr (St Audrie's Bay latest Rhaetian, cf. base of the Blue Lias Fm; see Ruhl *et al.*, 2010). In the Holy Cross Mountains (Niekłań section, SE Poland) marine flooding is marked by the onset of sandstones of parasequence IC (base of the Skłoby Fm). Astronomical calibration indicates that those were deposited ~600 kyr after the beginning of the Jurassic, arriving to Niekłań already during the Liassicus Zone (Fig. 3; see also Hesselbo *et al.*, 2002, 2004; Pieńkowski, 2004a; Barth *et al.*, 2018). Consequently, relative to NW Poland, it took another ~400 kyr until the brackish-marine transgression flooded the HCM region, some 600 km towards the south-east.

Magnitude of the 'Planorbis' transgression

Based on the orbital timeframe from the present study, one can attempt to estimate sedimentation rates, development of accommodation space, and scale of related sea-level rise. Characteristic is much different thickness of eccentricity cycle e1 compared to cycles e2–e7 (Fig. 6). The relatively thick e1 cycle translates into sedimentation rate of about 0.31 m/kyr. In turn, the succeeding cycles e3–e7 manifest comparable thicknesses (e2: ~20.8 m; e3: 18.4 m; e4: ~14.9 m; e5: ~24.2 m; e6: ~18.3 m; e7: ~19.0 m) and deposition rates (0.15–0.24 m/kyr; mean: ~0.17 m/kyr).

Assuming that the sediment thickness and accommodation space in the 'lacustrine' e4 cycle was mostly created by subsidence, and that subsidence did not change significantly in time (Brański, 2006, 2014), the e4 cycle (the one with the lowest thickness) can be considered as reflecting a 'reference' of subsidence rate (~15 m / 100 kyr) during the Hettangian in the HCM sector of the Polish Basin. In that way one can attribute 'extra' accommodation space during other cycles mainly to global sea-level rise and associated rise of the base-level (Pieńkowski, 2004a). On that basis, an additional 16 m thickness of e1 cycle is thought reflect the mag-

nitude of sea-level rise; for cycles e2–e6 that would be another ~21 m. This gives a total 'excess' accommodation space of ~37 m. If rather limited burial of Hettangian in the HCM region (approximated here to ~1000 m; see Remin *et al*., 2022) and compaction factor of 1.5 (for mix of sandstones and shales; see Lee *et al.*, 2020) is also taken in account, early Hettangian transgression would result in sea-level rise of *ca.* 55 m, that is slightly more than previously estimated by Haq (2018; ~30–40 m). Noteworthy, in this case the subsidence rate calculation approach consumes also the issue of sediment loading factor, which mostly decreased during the Hettangian. That is because the early Hettangian climate aridization (relative to 'wet' late Rhaetian) most likely resulted in lowered rates of continental weathering, thus riverine input as well. This is also in agreement with mean sedimentation rates calculated for parasequences IA and IB, where parasequence IA is 55 m thick and covers two short eccentricity cycles (~0.275 m/kyr), while parasequence IB is 70 m thick and corresponds to four short eccentricity cycles (~0.175 m/kyr). Ultimately, the above calculations are not (or only limitedly) affected by 'missing' rock volume; erosional gaps in Niekłań PIG core result from syn-sedimentary processes, so that any additional accommodation from erosion space was likely filled soon after.

CONCLUSIONS

The base of the Hettangian in the Niekłań borehole is approximated by the FO of *C. thiergartii* (158 m). Palynological records provide evidence for two fern spikes, first in the uppermost Rhaetian and the second already within the Hettangian. These are interpreted as a manifestation of the stepwise (?bipartite) end-Triassic extinction. Carbon isotope ($\delta^{13}C_{WOOD}$) data from the uppermost Rhaetian–lower Hettangian of the Niekłań borehole enables detailed correlation with the 'main' CIE at the T–J boundary interval; this, in turn, allows to set the base of the Hettangian at 159 m of the section. Clay mineral assemblages, additionally supported by elemental geochemistry (CIA), sedimentologic observations and palynologic data allow inference of weathering regime and paleoclimate, that is: 1) seasonal and gradually more and more humid early–mid Rhaetian; 2) warm and humid late Rhaetian; 3) transient cooling at the T/J boundary; 4) arid earliest Hettangian; and 5) generally mild Hettangian. Astronomical calibration of the MS signal enabled recognition of seven 100 kyr short eccentricity cycles (e1–e7), which cover the interval of transition from fluvial to marine facies (so-called Planorbis marine transgression). The delay in marine flooding onto the HCM is approximated to ~700 kyr relative to SW Britain and ~400 kyr relative to NW Poland. Calculated sedimentation rates and subsidence estimations suggest that Planorbis transgression resulted in ~55 m rise of a sea-level, most of which occurred during the first 200 kyr of the Hettangian.

Acknowledgements. We thank Andrzej Szymkowiak and PhD Krystian Wójcik for help in collecting magnetic susceptibility data. We are thankful to prof. Jacek Grabowski for useful remarks concerning magnetic susceptibility. The authors are also grateful to Anne-Christine da Silva and Anna Becker for their careful reviews and important remarks, which allowed us to improve this paper. This research was financed from resources of the National Science Centre (Poland), grants no. DEC-2012/06/M/ST10/00478 and 2017/25/B/ST10/02235 (leader: Grzegorz Pieńkowski). MJL publishes with the approval of the Director, British Geological Survey (NERC). SPH acknowledges NERC grant (NE/N018508/1) and funding from the International Continental Scientific Drilling Program (ICDP) for the JET project (Integrated Understanding of the Early Jurassic Earth System and Timescale). RP was funded by a University of Exeter PhD studentship.

REFERENCES

AHLBERG A., OLSSON I., ŠIMKEVIČIUS P., 2003 – Triassic–Jurassic weathering and clay mineral dispersal in basement areas and sedimentary basins of southern Sweden. *Sedimentary Geology*, **161**: 15–29.

ARNDORFF L., 1993 – Lateral relations of deltaic palaeosols from the Lower Jurassic Rønne Formation on the island of Bornholm, Denmark. *Palaeogeography, Palaeoclimatology, Palaeoecology*, **100**: 235–250.

BARBACKA M., ZIAJA J., WCISŁO-LURANIEC E., 2010 – Taxonomy and palaeoecology of the Early Jurassic macroflora from Odrowąż, central Poland. *Acta Geologica Polonica*, **60**: 373–392.

BARTH G., PIEŃKOWSKI G., ZIMMERMANN J., FRANZ M., KUHLMANN G., 2018 – Palaeogeographical evolution of the Lower Jurassic: High-resolution biostratigraphy and sequence stratigraphy in the Central European Basin. *In*: Mesozoic Resource Potential in the Southern Permian Basin (Eds. B. Kilhams *et al.*). *Geological Society, London, Special Publications*, **469**: 341–369.

BARTOLINI A., GUEX J., SPANGENBERG J.E., SCHOENE B., TAYLOR D.G., SCHALTEGGER U., ATUDOREI V., 2012 – Disentangling the Hettangian carbon isotope record: Implications for the aftermath of the end-Triassic mass extinction. *Geochemistry, Geophysics, Geosystems*, **13**: 2011GC003807.

BEERLING D.J., BERNER R.A., 2002 – Biogeochemical constraints on the Triassic-Jurassic boundary carbon cycle event. *Global Biogeochemical Cycles*, **16**: 10-1–10-13.

BLACKBURN T.J., OLSEN P., BOWRING S.A., McLEAN N.M., KENT D.V., PUFFER J., MCHONE G.,

RASBURY E.T., ET-TOUHAMI M., 2013 – Zircon U–Pb geochronology links the end-Triassic extinction with the Central Atlantic Magmatic Province. *Science*, **340**: 931–945.

BLACKEY R., 2020 – Deep Time Maps. Europe Jurassic ca. 200 Ma. https://deeptimemaps.com

BLOOS G., 1976 – Untersuchungen über Bau and Entstehung der feinkornigen Sandsteine des Schwarzen Jura (Hettangium u. Tiefstes Sinemurium) im schwabischen Sedimentationsbereich. *Arbeiten aus dem Institut für Geologie und Paläontologie an der Universität Stuttgart*, **71**: 1–269.

BONIS N.R., KURSCHNER W.M., KRYSTYN L., 2009 – A detailed palynological study of the Triassic–Jurassic transition in key sections of the Eiberg Basin (Northern Calcareous Alps, Austria). *Review of Palaeobotany and Palynology*, **156**: 376–400.

BONIS N.R., RUHL M., KURSCHNER W.M., 2010 – Climate change driven black shale deposition during the end-Triassic in the western Tethys. *Palaeogeography, Palaeoclimatology, Palaeoecolpgy*, **290**: 151–159.

BOS R., ZHENG W., LINDSTRÖM S., SENEI H., WAAJEN I., FENDLEY I.M., MATHER T.A., WANG Y., ROHOVEC J., NAVRÁTIL T., SLUIJS A., van de SCHOOTBRUGGE B., 2024 – Climate forced Hg-remobilization associated with fern mutagenesis in the aftermath of the end-Triassic extinction. *Nature Communications*, **15**: 3596.

BRAŃSKI P., 2006 – Lower Hettangian in the Holy Cross Mountains region – an example of tectonically-controlled sedimentation in the epicontinental basin of Poland. *Volumina Jurassica*, **4**: 80–81.

BRAŃSKI P., 2014 – Climatic disaster at the Triassic–Jurassic boundary – a clay minerals and major elements record from the Polish Basin. *Gelogical Quarterly*, **58**: 291–310.

CLEVELAND W.S., 1979 – Robust locally weighted regression and smoothing scatterplots. *Journal of the American Statistical Association*, **74**: 829–836.

COE A.L., HESSELBO S.P., 2000 – Discussion of Hallam (1999). "Evidence of sea-level fall in sequence stratigraphy: Examples from the Jurassic". *Geology*, **28**: 95.

DECKONINCK J.-F., HESSELBO S.P., DEBUISSER N., AVERBUCH O., BAUDIN F., BESSA J., 2003 – Environmental controls on clay mineralogy of an Early Jurassic mudrock (Blue Lias Formation, southern England). *International Journal of Earth Sciences*, **92**: 255–266.

DEENEN M.H.L., RUHL M., BONIS N.R., KRIJGSMAN W., KUERSCHNER W.M., REITSMA M., van BERGEN M.J., 2010 – A new chronology of the end-Triassic mass extinction. *Earth and Planetary Science Letters*, **291**: 113–125.

FEIST-BURKHARDT S., GÖTZ A.E., SZULC J., BORKHATARIA R., GELUK M., HAAS J., HORNUNG J., JORDAN P., KEMPF O., MICHALÍK J., NAWROCKI J., REINHARDT L., RICKEN W., RÖHLING H.-G., RÜFFER T., TÖRÖK Á., ZÜHLKE R., 2008 – Triassic. *In*: The Geology of Central Europe Volume 2: Mesozoic and Cenozoic, (Ed. T McCann): 749–823. *Geological Society of London*, London.

FOX C.P., WHITESIDE J.H., OLSEN P.E., CUI X., SUMMONS R.E., IDIZ E., GRICE K., 2021 – Two-pronged kill mechanism at the end-Triassic mass extinction. *Geology*, **50**: 448–453.

GANINO C., ARNDT N., 2009 – Climate changes caused by degassing of sediments during the emplacement of large igneous provinces. *Geology*, **37**: 323–326.

GOTZ A.E., RUCKWIED K., PALFY J., HAAS J., 2009 – Palynological evidence of synchronous changes within the terrestrial and marine realm at the Triassic/Jurassic boundary (Csővar section, Hungary). *Review of Palaeobotany and Palynolgy*, **156**: 401–409.

GRAVENDYCK J., COIFFARD C., BACHELIER J.B., KÜRSCHNER W., 2023 – Re-evaluation of *Cerebropollenites thiergartii* Eberh.Schulz 1967 and related taxa: priority of *Sciadopityspollenites* and nomenclatural novelties. *Grana*, **62**: 1–47.

GREENE S.E., BOTTJER D.J., CORSETTI F.A., BERELSON W.M., ZONNEVELD J.-P., 2012 – A subseafloor carbonate factory across the Triassic-Jurassic transition. *Geology*, **40**: 1043–1046.

GUEX J., BARTOLINI A., ATUDOREI V., TAYLOR D., 2004 – High-resolution ammonite and carbon isotope stratigraphy across the Triassic–Jurassic boundary at New York Canyon (Nevada). *Earth and Planetary Science Letters*, **225**: 29–41.

HALBRITTER H., ULRICH S., GRÍMSSON F., WEBER M., ZETTER R., HESSE M., BUCHNER R., SVOJTKA M., FROSCH-RADIVO A., 2018 – Methods in Palynology. *In*: Illustrated Pollen Terminology: 99–127. Springer, Cham.

HALLAM A., 1997 – Estimates of the amount and rate of sea-level change across the Rhaetian–Hettangian and Pliensbachian–Toarcian boundaries (latest Triassic to Early Jurassic). *Journal of Geological Society, London*, **154**: 773–779.

HALLAM A., 2001 – A review of the broad pattern of Jurassic sea-level changes and their possible causes in the light of current knowledge. *Palaeogeography, Palaeoclimatology, Palaeoecology*, **147**: 23–37.

HALLAM A., WIGNALL P.B., 1999 – Mass extinctions and sea-level changes. *Earth Science Reviews*, **48**: 217–250.

HAQ B.U., 2017 – Triassic eustatic variations re-examined. *GSA Today*, **28**: GSATG381A.1

HAQ B.U., 2018 – Jurassic sea-level variations: A reappraisal. *GSA Today*, **28**: 4–10.

HAUTMANN M., STILLER F., HUAWEI C., JINGENG S., 2008 – Extinction-recovery pattern of level-bottom faunas across the Triassic-Jurassic boundary in Tibet: Implications for potential killing mechanisms. *Palaios*, **23**: 711–718.

HEIMDAL T.H., JONES M.T., SVENSEN H.H., 2020 – Thermogenic carbon release from the Central Atlantic magmatic province caused major end-Triassic carbon cycle perturbations. *Proceedings of the National Academy of Sciences*, **117**: 11968–11974.

HESSELBO S.P., GRÖCKE D.R., JENKYNS H.C., BJERRUM C.J., FARRIMOND P,. MORGANS-BELL H.S., GREEN O.R., 2000 – Massive dissociation of gas hydrate during a Jurassic oceanic anoxic event. *Nature*, **406**: 392–395.

HESSELBO S.P., ROBINSON S.A., SURLYK F., PIASECKI S., 2002 – Terrestrial and marine extinction at the Triassic–Jurassic boundary synchronized with major carbon-cycle perturbation: A link to initiation of massive volcanism? *Geology*, **30**: 251–254.

HESSELBO S.P., ROBINSON S.A., SURLYK F., 2004 – Sea-level change and facies development across potential Triassic–

Jurassic boundary horizons, SW Britain. *Journal of Geological Society*, **161**: 365–379.

HESSELBO S.P., McROBERTS C.A., PÁLFY J., 2007 – Triassic–Jurassic boundary events: Problems, progress, possibilities. *Palaeogeography, Palaeoclimatology, Palaeoecology*, **244**: 1–10.

HESSELBO S.P., AL-SUWAIDI A., BAKER S., BALLABIO G., BELCHER C.M., BOND A., BOOMER I., BJERRUM C.J., BOGUS K., BOYLE R., BROWNING J.V., BUTCHER A.R., CONDON D.J., COPESTAKE P., DAINES S., DALBY C., DAMASCHKE M., DAMBORENEA S.E., DECONINCK J.-F., DICKSON A.J., FENDLEY I.M., FOX C.P., FRAGUAS A., FRIELING J., GIBSON T.A., HE T., HICKEY K., HINNOV L.A., HOLLAAR T.P., HUANG C., HUDSON A.J.L., JENKYNS H.C., IDIZ E., JIANG M., KRIJGSMAN W., KORTE C., LENG M.J., LENTON T.M., LEU K., LITTLE C.T.S., MACNIOCAILL C., MANCEÑIDO M.O., MATHER T.A., MATTIOLI E., MILLER K.G., NEWTON R.J., PAGE K.N., PÁLFY J., PIEŃKOWSKI G., PORTER R.J., POULTON S.W., RICCARDI A.C., RIDING J.B., ROPER A., RUHL M., SILVA R.L., STORM M.S., SUAN G., SZŰCS D., THIBAULT N., UCHMAN A., STANLEY J.N., ULLMANN C.V., van de SCHOOTBRUGGE B., VICKERS M.L., WADAS S., WHITESIDE J.H., WIGNALL P.B., WONIK T., XU W., ZEEDEN C., ZHAO K., 2023 – Initial results of coring at Prees, Cheshire Basin, UK (ICDP JET project): Towards an integrated stratigraphy, timescale, and Earth system understanding for the Early Jurassic. *Scientific Drilling*, **32**: 1–25.

HILLEBRANDT A.V., KRYSTYN L., KURSCHNER W.M., BONIS N.R., RUHL M., RICHOZ S., SCHOBBEN M.A.N., URLICHS M., BOWN P.R., KMENT K., McROBERTS C.A., SIMMS M., TOMASOVYCH A., 2013 – The Global Stratotype Sections and Point (GSSP) for the Base of the Jurassic System at Kuhjoch (Karwendel Mountains, Northern Calcareous Alps, Tyrol, Austria). *Episodes*, **36**: 162–198.

HOUNSLOW M.W., POSEN P.E., WARRINGTON G., 2004 – Magnetostratigraphy and biostratigraphy of the upper Triassic and lowermost Jurassic succession, St Audrie's Bay, UK. *Palaeogeography, Palaeoclimatology, Palaeoecology*, **213**: 331–358.

JOVANE L., SPROVIERI M., FLORINDO F., ACTON G., COCCIONI R., DALL'ANTONIA B., DINARÈS-TURELL J., 2007 – Eocene-Oligocene paleoceanographic Changes in the stratotype section, Masasignano, Italy: Clues from rock magnetism and stable isotopes. *Journal of Geophysical Research*, **112**: B11101.

KORTE C., HESSELBO S.P., JENKYNS H.C., RICKABY R.E.M., SPÖTL C., 2009 – Palaeoenvironmental significance of carbon- and oxygen-isotope stratigraphy of marine Triassic/Jurassic boundary sections in SW Britain. *Journal of the Geological Society*, **166**: 431–445.

LARSSON L.M., 2009 – Palynostratigraphy of the Triassic–Jurassic transition in southern Sweden. *Journal of the Geological Society of Sweden*, **131**: 147–163.

LEE E.Y., NOVOTNY J., WAGREICH M., 2020 – Compaction trend estimations and applications to sedimentary basin reconstruction (BasinVis 2.0). *Applied Computing and Geosciences*, **5**: 100015.

LEU K., ZEEDEN C., ULFERS A., ABADI M.S., VINNEPAND M., RUHL M., HESSELBO S., WONIK T., 2024 – Astronomical calibration of teh Early Jurassic Sinemurian Stage based on cyclostratigraphic studies of downhole logging data in the Prees 2 borehole (Cheshire Basin, UK). *Newsletters on Stratigraphy*, **57**: 257–282.

LI M.S., ZHANG Y., HUANG C.J., OGG J., HINNOV L., WANG Y.D., ZOU Z.Y., LI L.Q., 2017 – Astronomical tuning and magnetostratigraphy of the Upper Triassic Xujiahe Formation of South China and Newark Supergroup of North America: Implications for the Late Triassic time scale. *Earth and Planetary Science Letters*, **475**: 207–223.

LINDSTRÖM S., 2021 – Two-phased mass rarity and extinction in land plants during the end-Triassic Climate Crisis. *Frontiers in Earth Sciences*, **9**: 1079.

MANN M.E., LEES J.M., 1996 – Robust estimation of background noise and signal detection in climatic time series. *Climatic Change*, **33**: 409–445.

MARCINKIEWICZ T., 1962 – Rhaetian and Lias megaspores from borehole Mechowo near Kamień Pomorski and their stratigraphical value. *Prace Państwowego Instytutu Geologicznego*, **30**: 469–493.

MARCINKIEWICZ T., 1971 – The stratigraphy of the Rhaetian and Lias in Poland based on megaspore investigations. *Prace Państwowego Instytutu Geologicznego*, **65**: 1–58.

MAREK S., PAJCHLOWA M., 1997 – The epicontinental Permian and Mesozoic in Poland. *Prace Państwowego Instytutu Geologicznego*, **153**.

MARTINEZ M., DECONINCK J.-F., PELLENARD P., RIQUIER L., COMPANY M., REBOULET S., MOIROUD M., 2015 – Astrochronology of the Valanginian–Hauterivian stages (Early Cretaceous): Chronological relationships between the Paraná–Etendeka large igneous province and the Weissert and the Faraoni events. *Global and Planetary Change*, **131**: 158–173.

MARZOLI A., BERTRAND H., KNIGHT K.B., CIRILLI S., BURAATTI N., VÉRATI C., NOMADE S., RENNE P.R., YOUBI N., MARTINI R., ALLENBACH K., NAUWERTH R., RAPAILLE C., ZANINETTI L., BELIENI G., 2004 – Synchrony of the Central Atlantic magmatic province and the Triassic-Jurassic boundary climatic and biotic crisis. *Geology*, **32**: 973–976.

McELWAIN J.C., BEERLING D.J., WOODWARD F.I., 1999 – Fossil plants and global warming at the Triassic–Jurassic boundary. *Science*, **285**: 1386–1390.

McLENNAN S.M., 1993 – Weathering and global denudation. *Journal of Geology*, **101**: 2095–303.

MEYERS S.R., SAGEMAN B.B., 2004 – Detection, quantification, and significance of hiatuses in pelagic and hemipelagic strata. *Earth and Planetary Science Letters*, **224**: 55–72.

MOORE D.M., REYNOLDS R.C., 1997 – X-ray diffraction and identification and analysis of clay minerals. 2nd Edition. Oxford University Press, New York.

NESBITT H.W., YOUNG G.M., 1982 – Early Proterozoic climates and plate motions inferred from major element chemistry of lutites. *Nature*, **299**: 715–717.

NIEDŹWIEDZKI G., 2011 – Dinosaur tracks from the Early Jurassic ecosystem of Sołtyków, Holy Cross Mountains. *Biuletyn Państwowego Instytutu Geologicznego*, **447**: 49–98.

OLSEN P.E., KENT D.V., SUES H.D., KOEBERL C., HUBER H., MONTANARI A., RAINFORTH E.C., FOWELL S.J., SZAJNA M.J., HARTLINE B.W., 2002 – Ascent of dinosaurs linked to an iridium anomaly at the Triassic–Jurassic boundary. *Science*, **296**: 1305–1307.

OPDYKE N.D., CHANNELL J.E.T., 1996 – Magnetic stratigraphy. Academic Press, San Diego.

PÁLFY J., DEMENY A., HAAS J., HTENYI M., ORCHARD M.J., VETO I., 2001 – Carbon isotope anomaly at the Triassic–Jurassic boundary from a marine section in Hungary, *Geology*, **29**: 1047–1050.

PIEŃKOWSKI G., 1991 – Eustatically-controlled sedimentation in the Hettangian–Sinemurian (Early Jurassic) of Poland and Sweden. *Sedimentology*, **38**: 503–518.

PIEŃKOWSKI G., 1997 – Jura dolna. Litostratygrafia i litofacje. Sedymentacja i stratygrafia sekwencji liasu w Polsce na podstawie wybranych profilów. *In*: The epicontinental Permian and Mesozoic in Poland (Eds. S. Marek, M. Pajchlowa). *Prace Państwowego Instytutu Geologicznego*, **53**: 217–236 [in Polish with English summary].

PIEŃKOWSKI G., 2004a – The epicontinental Lower Jurassic of Poland. *Polish Geological Institute Special Papers*, **12**: 1–154.

PIEŃKOWSKI G., 2004b – Sołtyków, Poland – an unique palaeoecologiacl record of the Early Jurassic continental deposits. *Volumina Jurassica*, **2**: 1–16 [in Polish with English abstract].

PIEŃKOWSKI G., 2009 – Trias. Polska pozakarpacka. *In*: Suplement do Tabeli Stratygraficznej Polski (Ed. R. Wagner): 50–51. Państwowy Instytut Geologiczny – Państwowy Instytut Badawczy, Warszawa [in Polish].

PIEŃKOWSKI G., WAKSMUNDZKA M., 2009 – Palynofacies in Lower Jurassic epicontinental deposits of Poland: Tool to interpret sedimentary environments. *Episodes*, **32**: 21–32.

PIEŃKOWSKI G., NIEDŹWIEDZKI G., WAKSMUNDZKA M., 2012 – Sedimentological, palynological and geochemical studies of the terrestrial Triassic–Jurassic boundary in northwestern Poland. *Geological Magazine*, **149**: 308–332.

PIEŃKOWSKI G., NIEDŹWIEDZKI G., BRAŃSKI P., 2014 – Climatic reversals related to the Central Atlantic magmatic province caused the end-Triassic biotic crisis – Evidence from continental strata in Poland. *Geological Society of America Special Papers*, **505**: 263–286.

PIEŃKOWSKI G., HESSELBO S.P., BARBACKA M., LENG M.J., 2020 – Non-marine carbon-isotope stratigraphy of the Triassic-Jurassic transition in the Polish Basin and its relationships to organic carbon preservation, pCO_2 and palaeotemperature. *Earth-Science Reviews*, **210**: 103383.

PRETO N., KUSTATSCHER E., WIGNALL P.B., 2010 – Triassic climates – State of the art and perspectives. *Palaeogeography, Palaeoclimatology, Palaeoecology*, **290**: 1–10.

REMIN Z., CYGLICKI M., NIECHWEDOWICZ M., 2022 – Deep vs. shallow – two contrasting theories? A tectonically activated Late Cretaceous deltaic system in the axial part of the Mid-Polish Trough: A case study from southeast Poland. *Solid Earth*, **13**: 681–703.

REYMANÓWNA M., 1992 – Two conifers from the Liassic flora of Odrowąż in Poland. *In*: Palaeovegetational development in Europe and regions relevant to its palaeofloristic evolution (Ed. J. Kovar-Eder): 307–311. *Proceedings Pan-European Palaeobotanical Conference*. Museum of Natural History, Vienna.

RUHL M., KÜRSCHNER W.M., 2011 – Multiple phases of carbon cycle disturbance from large igneous province formation at the Triassic-Jurassic transition. *Geology*, **39**: 431–434.

RUHL M., KÜRSCHNER W.M, KRYSTYN L., 2009 – Triassic–Jurassic organic carbon isotope stratigraphy of key sections in the western Tethys realm (Austria). *Earth and Planetary Science Letters*, **281**: 169–187.

RUHL M., DEENEN M.H.L., ABELS H.A., BONIS N.R., KRIJGSMAN W., KÜRSCHNER W.M., 2010 – Astronomical constraints on the duration of the early Jurassic Hettangian stage and recovery rates following the end-Triassic mass extinction (St Audrie's Bay/East Quantoxhead, UK). *Earth and Planetary Science Letters*, **295**: 262–276.

RUHL M., HESSELBO S.P., HINNOV L., JENKYNS H.C., XU W., RIDING J.B., STORM M., MINISINI D., ULLMANN C.V., LENG M.J., 2016 – Astronomical constraints on the duration of the Early Jurassic Pliensbachian Stage and global climatic fluctuations. *Earth and Planetary Science Letters*, **455**: 149–165.

RUHL M., HESSELBO S.P., AL-SUWAIDI A., JENKYNS H.C., DAMBORENEA S.E., MANCEÑIDO M.O., STORM M., MATHER T.A., RICCARDI A.C., 2020 – On the onset of Central Atlantic Magmatic Province (CAMP) volcanism and environmental and carbon-cycle change at the Triassic–Jurassic transition (Neuquén Basin, Argentina). *Earth-Science Reviews*, **208**: 103229.

SCHALLER M.F., WRIGHT J.D., KENT D.V., 2011 – Atmospheric PCO_2 perturbations associated with the Central Atlantic Magmatic Province. *Science*, **331**: 1404–1409.

SCHALLER M.F., WRIGHT J.D., KENT D.V., OLSEN P.E., 2012 – Rapid emplacement of the Central Atlantic magmatic province as a net sink for CO_2. *Earth and Planetary Science Letters*, **323/324**: 27–39.

SCHALTEGGER U., GUEX J., BARTOLINI A., SCHOENE B., OVTCHAROVA M., 2008 – Precise U–Pb age constraints for end-Triassic mass extinction, its correlation to volcanism and Hettangian post-extinction recovery. *Earth and Planetary Science Letters*, **267**: 266–275.

SCHOENE B., GUEX J., BARTOLINI A., SCHALTEGGER U., BLACKBURN T.J., 2010 – Correlating the end-Triassic mass extinction and flood basalt volcanism at the 100 ka level. *Geology*, **38**: 387–390.

SCHOOTBRUGGE B. van de, QUAN T.M., LINDSTROM S., PUTTMANN W., HEUNISCH C., PROSS J., FIEBIG J., PETSCHICK R., ROHLING H.-G., RICHOZ S., ROSENTHAL Y., FALKOWSKI P.G., 2009 – Floral changes across the Triassic/Jurassic boundary linked to flood basalt volcanism. *Nature Geoscience*, **2**: 589–594.

SCHOOTBRUGGE B. van de, WEIJST C.M.H. van der, HOLLAAR T.P., VECOLI M., STROTHER P.K., KUHLMANN N., THEIN J., VISSCHER H., van KONIJNENBURG-van CITTERT H., SCHOBBEN M.A.N., SLUIJS A., LINDSTRÖM S., 2020 – Catastrophic soil loss associated

with end-Triassic deforestation. *Earth-Science Reviews*, **210**: 103332.

SHA J., VAJDA V., PAN Y., LARSSON L., YAO X., ZHANG X., WANG Y., CHENG X., JIANG B., DENG S., CHEN S., PENG B., 2011 – Stratigraphy of the Triassic-Jurassic boundary successions of the southern margin of the Junggar Basin, northwestern China. *Acta Geologica Sinica*, **85**: 421–436.

SHA J., OLSEN P.E., PAN Y., XU D., WANG Y., ZHANG X., YAO X., VAJDA V., 2015 – Triassic–Jurassic climate in continental high-latitude Asia was dominated by obliquity-paced variations (Junggar Basin, Ürümqi, China). *Proceedings of the National Academy of Sciences*, **112**: 3624–3629.

STEINHORSDOTTIR M., JERAM A.J., McELWAIN J.C., 2011 – Extremely elevated CO_2 concentrations at the Triassic/Jurassic boundary. *Palaeogeography, Palaeoclimatology, Palaeoecology*, **308**: 418–432.

STORM M.S., HESSELBO S.P., JENKYNS H.C., RUHL M., ULLMANN C.V., XU W., LENG M.J., RIDING J.B., GORBANENKO O., 2020 – Orbital pacing and secular evolution of the Early Jurassic carbon cycle. *Proceedings of the National Academy of Sciences*, **117**: 3974–3982.

ŚRODOŃ J., 2006 – Identification and quantitative analysis of clay minerals. *In:* Handbook of Clay Science (Eds. F. Bergaya *et al.*). Chapter 12.4. *Elsevier*.

THOMSON D.J., 1982 – Spectrum estimation and harmonic analysis. *Proceedings of the IEEE*, **70**: 1055–1096.

THOMSON D.J., 1990 – Quadratic-inverse spectrum estimates: Applications to palaeoclimatology. *Philosophical Transactions of the Royal Society of London Series A*, **332**: 539–597.

TRIBOVILLARD N., ALGEO T.J., LYONS T., RIBOULLEAU A., 2006 – Trace metals as paleoredox and paleoproductivity proxies: An update. *Chemical Geology*, **232**: 12–32.

VAJDA V., CALNER M., AHLBERG A., 2013 – Palynostratigraphy of dinosaur footprint-bearing deposits from the Triassic–Jurassic boundary interval of Sweden. *Journal of the Geological Society of Sweden*, **135**: 120–130.

VENUTI A., FLORINDO F., MICHEL E., HALL I.R., 2007 – Magnetic proxy for deep (Pacific) western boundary current variability across the mid-Pleistocene climate transition. *Earth and Planetary Science Letters*, **259**: 107–118.

WAGNER R., 2008 – Stratigraphical Table of Poland. Polish Geological Institute. ISBN 978-83-7538-426-0.

WARD P.D., HAGGART J.W., CARTER E.S., WILBUR D., TIPPER H.W., EVANS T., 2001 – Sudden productivity collapse associated with the Triassic–Jurassic boundary mass extinction. *Science*, **292**: 1148–1151.

WARRINGTON G., COPE J.C.W., IVIMEY-COOK H.C., 2008 – The St Audrie's Bay – Doniford Bay section, Somerset, England: Updated proposal for a candidate Global Stratotype Section and Point for the base of the Hettangian Stage, and of the Jurassic System. *International Subcommission on Jurassic Stratigraphy Newsletter*, **35**: 2–66.

WEEDON G.P., JENKYNS H.C., COE A.L., HESSELBO S.P., 1999 – Astronomical calibration of the Jurassic time-scale from cyclostratigraphy in British mudrock formations. *Philosophical Transactions of the Royal Society of London*, **357**: 1787–1813.

WEEDON G.P., PAGE K.N., JENKYNS H.C., 2019 – Cyclostratigraphy, stratigraphic gaps and the duration of the Hettangian stage (Jurassic): Insights from the Blue Lias Formation of southern Britain. *Geological Magazine*, **156**: 1469–1509.

WEEMS R.E., LUCAS S.G., 2015 – A revision of the Norian conchostracan zonation in North America and its implications for Late Triassic North American tectonic history. *New Mexico Museum of Natural History and Science Bulletin*, **67**: 303–317.

WHITESIDE J.H., OLSEN P.E., KENT D.V., FOWELL S.J., ET-TOUHAMI M., 2007 – Synchrony between the Central Atlantic magmatic province and the Triassic–Jurassic mass-extinction event? *Palaeogeography, Palaeoclimatology, Palaeoecology*, **244**: 345–367.

WHITESIDE J.H., OLSEN P.E., TIMOTHY I., EGLINTON T.I., CORNET B., McDONALD N.G., HUBER P., 2011 – Pangean great lake paleoecology on the cusp of the end-Triassic extinction. *Palaeogeography, Palaeoclimatology, Palaeoecology*, **301**: 1–17.

WHITTAKER A., GREEN G.W., 1983 – Geology of the country around Weston-super-Mare. *Memoirs of the British Geological Survey*, London. Geological sheet 279 with parts of sheets 263 and 295.

WIGNALL P.B., ATKINSON J.W., 2020 – A two-phase end-Triassic mass extinction. *Earth-Science Reviews*, **208**: 103282.

WIGNALL P.B., BOND D.P.G., 2008 – The end-Triassic and early Jurassic mass extinction records in the British Isles. *Proceedings of the Geologists' Association*, **119**: 73–84.

ZIAJA J., 2006 – Lower Jurassic spores and pollen grains from Odrowąż, Mesozoic margin of the Holy Cross Mountains, Poland. *Acta Palaeobotanica*, **46**: 3–83.

Plates

PLATE 1

Core photographs from the lowermost part of the Niekłań PIG core

Box 186 (186–185 m): playa deposits of the Norian Zbąszynek beds

Box 184 (184–183 m): Norian/Rhaetian boundary (boundary between Zbąszynek beds and the ‘variegated’ Parszów beds)

Box 174 (174–173 m): fluvial mudstones of the ‘variegated’ Parszów beds (Rhaetian)

Box 164 (164–163 m): weathered colluvium of the ‘gray’ Parszów beds (upper Rhaetian)

Damian G. Lodowski *et al*. – Timing and duration of the early Hettangian marine inundation in the Polish Basin: Organic carbon isotopes and astronomical calibration of the Triassic–Jurassic transition of the Niekłań PIG core (Holy Cross Mountains, SE Poland)

PLATE 2

Core photographs from lower and middle part of the Niekłań PIG core

Box 162 (162–161 m): boundary between the ‘gray’ Parszów beds and the Zagaje Formation (uppermost Rhaetian)

Box 119 (119–118 m): fluvial deposits of the Zagaje Fm (lower Hettangian, parasequence IA)

Box 97 (97–98 m): lacustrine mudstones of the Zagaje Fm (lower Hettangian, parasequence IB)

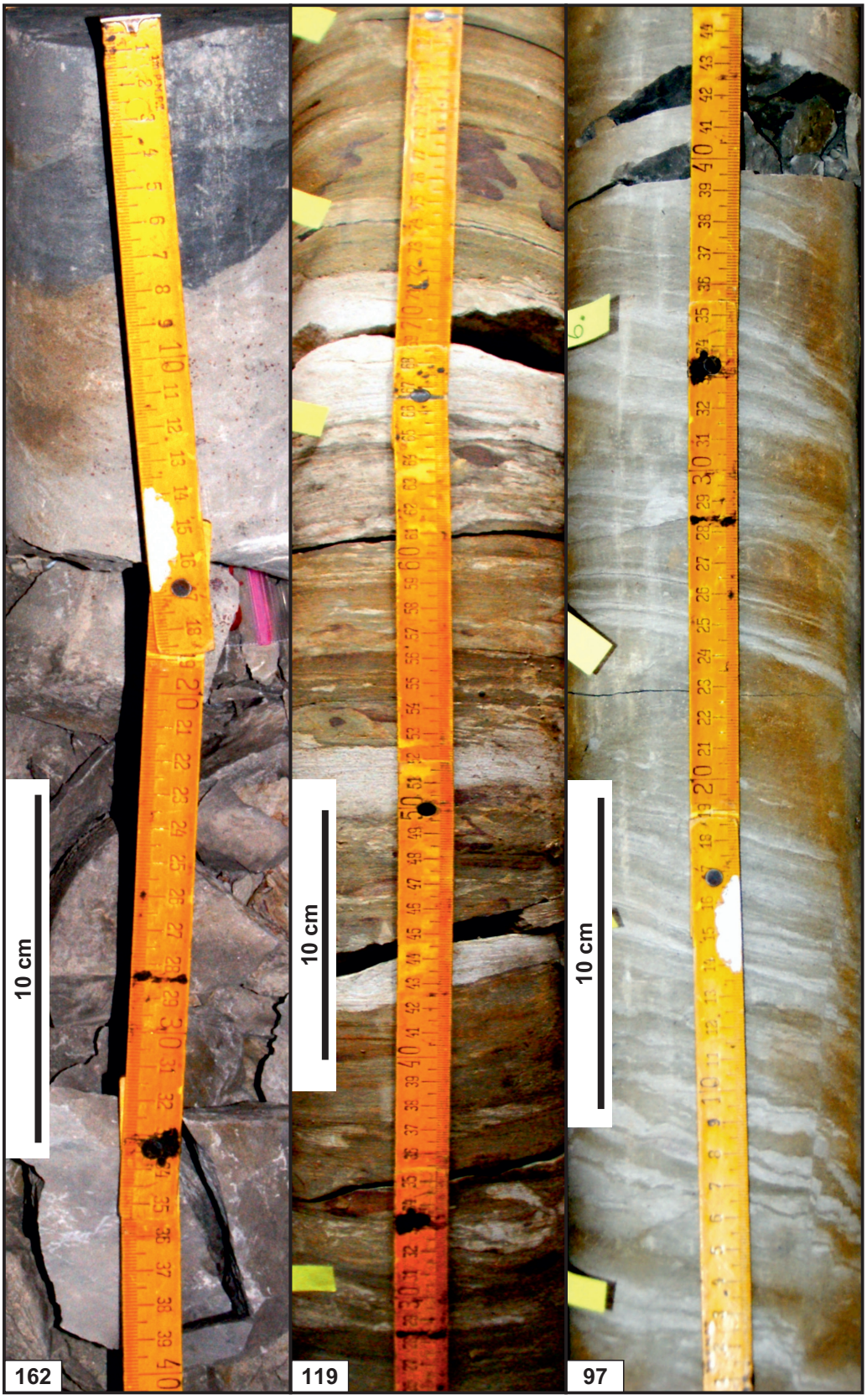

Damian G. Lodowski *et al*. – Timing and duration of the early Hettangian marine inundation in the Polish Basin: Organic carbon isotopes and astronomical calibration of the Triassic–Jurassic transition of the Niekłań PIG core (Holy Cross Mountains, SE Poland)

PLATE 3

Core photographs from upper part of the Niekłań PIG core

Box 57 (57–56 m): lacustrine sandstones and mudstones of the Zagaje Fm (middle Hettangian, parasequence IB)

Box 31 (31–30 m): boundary between the Zagaje Fm. and the Skłoby Fm (middle Hettangian, boundary between parasequences IB and IC)

Box 18 (18–17 m): marine mudstones of the Skłoby Fm (middle Hettangian, parasequence ID)

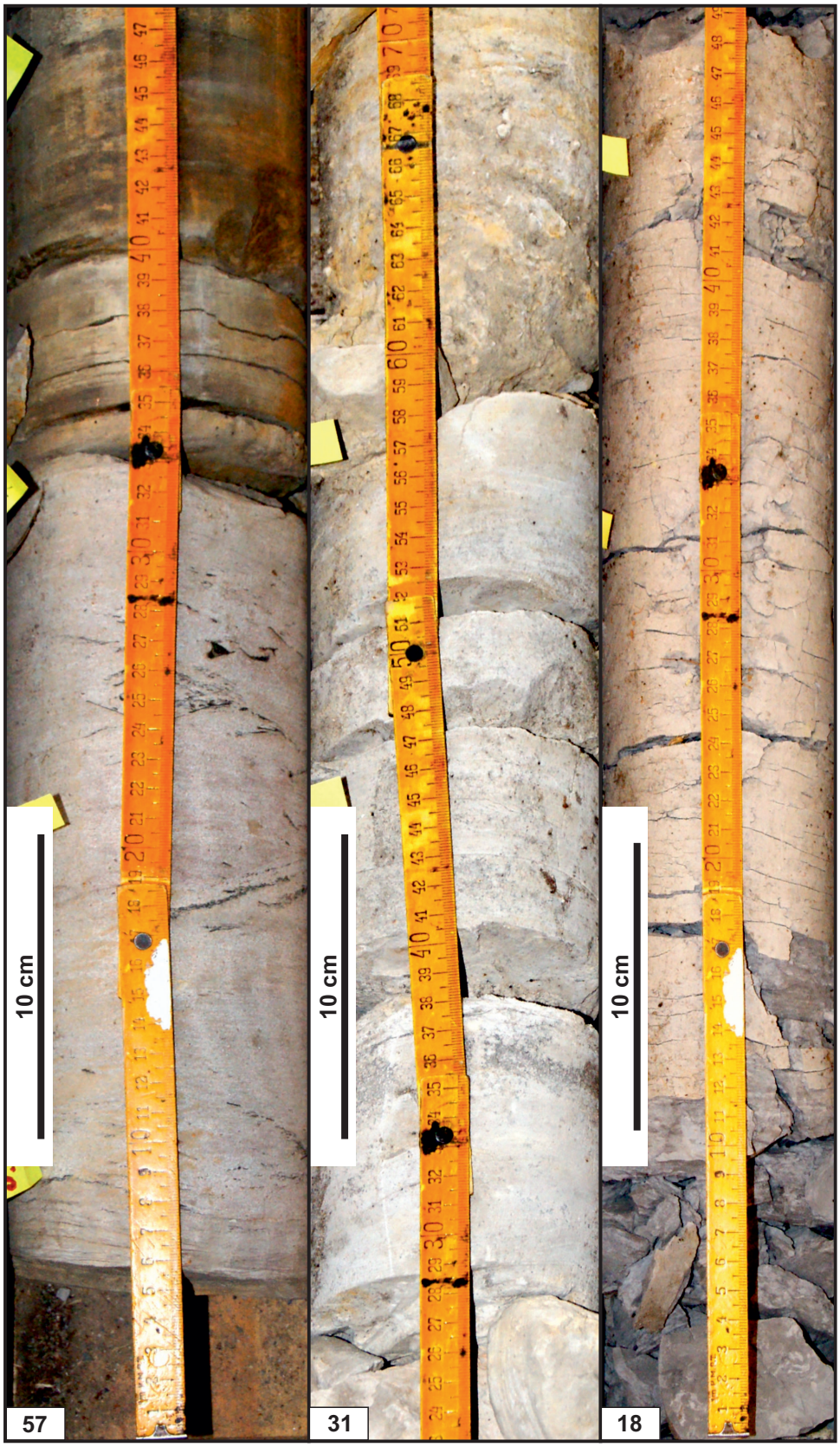

Damian G. Lodowski *et al*. – Timing and duration of the early Hettangian marine inundation in the Polish Basin: Organic carbon isotopes and astronomical calibration of the Triassic–Jurassic transition of the Niekłań PIG core (Holy Cross Mountains, SE Poland)